Geophys. J. Int. (2006) **165,** 565–583 doi: 10.1111/j.1365-246X.2006.02897.x

Imaging subduction from the trench to 300 km depth beneath the central North Island, New Zealand, with *Vp* and *Vp/Vs*

Martin Reyners,[1] Donna Eberhart-Phillips,[2] Graham Stuart[3] and Yuichi Nishimura[4]

[1] *GNS Science,* PO Box 30368, *Lower Hutt, New Zealand. E-mail: m.reyners@gns.cri.nz*
[2] *GNS Science, Private Bag* 1930, *Dunedin, New Zealand*
[3] *School of Earth Sciences, University of Leeds, Leeds* LS2 9JT, *UK*
[4] *Institute of Seismology & Volcanology, Hokkaido University,* N10 W8 *Kita-ku, Sapporo* 060-0810, *Japan*

Accepted 2005 December 31. Received 2005 November 16; in original form 2005 March 9

SUMMARY

Recent dense deployments of portable digital seismographs have provided excellent control on earthquakes beneath the central North Island of New Zealand. Here we use a subset of the best-recorded earthquakes in an inversion for the 3-D *Vp* and *Vp*/*Vs* structure. The data set includes 39 123 *P* observations and 18 331 *S* observations from 1239 earthquakes and nine explosions. The subducted plate is imaged as a high *Vp*, low *Vp*/*Vs* feature. *Vp* within the mantle of the subducted slab is almost always >8.5 km s^{-1}, which requires the *ca.* 120 Myr slab to be unusually cold. The low *Vp*/*Vs* within the subducted plate closely parallels the lower plane of the dipping seismic zone. It most likely indicates fluid resulting from dehydration of serpentine in the slab mantle, and the earthquakes themselves are likely to be promoted by dehydration embrittlement. We identify a region with $Vp < 8.0$ km s^{-1} which coincides with the upper plane of the dipping seismic zone and extends to *ca.* 65 km depth with the subducted Hikurangi Plateau, which is about 17 km thick prior to subduction. The mantle wedge is generally imaged as a low *Vp*, high *Vp*/*Vs* feature. However, there are significant changes evident in the wedge along the strike of the subduction zone. The region where *Vp* is lowest (7.4 km s^{-1}) and *Vp*/*Vs* is highest (1.87) occurs at 65 km depth, immediately west of the Taupo caldera. This region is best interpreted as a significant volume of partial melt, produced by the reaction of fluid released by dehydration of the subducted plate with the convecting mantle wedge. The region with lowest *Vp*, while paralleling the underlying dipping seismic zone, is located about 30 km from the upper surface of the zone. Material with $Vp >$ 8.0 km s^{-1} directly above the dipping seismic zone can be interpreted as sinking, entrained with the motion of the subducted slab and forming a viscous blanket that insulates the slab from the high-temperature mantle wedge. Material in the overlying low *Vp* region can be interpreted as rising within a return flow within the wedge. The volcanic front appears to be controlled by where this dipping low *Vp* region meets the base of the crust. The thickness of the backarc crust also shows significant variation along strike. In the central Taupo Volcanic Zone (TVZ) the crust is *ca.* 35 km thick, while southwest of Mt Ruapehu the crust thickens by *ca.* 10 km. There is no significant low *Vp* zone in the mantle wedge in this southwestern region, suggesting that this thicker crust has choked off mantle return flow. The seismic tomography results, when combined with constraints on mantle flow from previous shear-wave splitting results, provide a plausible model for both the distribution of volcanism in the central North Island, and the exceptional magmatic productivity of the central TVZ.

Key words: crustal structure, magmatism, mantle wedge, New Zealand, seismic velocity, subduction.

INTRODUCTION

Rapid lateral changes in subduction style occur in the central North Island of New Zealand. In the forearc, both seismological and GPS data suggest a southward increase in interseismic coupling at the seismogenic portion of the plate interface (Reyners 1998; Wallace *et al.* 2004). This results in a clockwise rotation of the forearc, which is accommodated in the backarc by extension of the Taupo Volcanic Zone (TVZ) in the north, and by compression of the Wanganui Basin in the south (Fig. 1). At the same time, subduction

in the central North Island is modified by the Hikurangi Plateau, a large igneous province on the incoming Pacific plate (Mortimer & Parkinson 1996). This plateau has a crustal thickness of about 17 km to the east of the central North Island (Davy & Wood 1994), and the buoyancy of the subducted plateau has resulted in exposure of the forearc above the shallow part of the subduction thrust.

The central North Island thus affords an excellent opportunity to study a complete downdip section of the Hikurangi subduction zone, and also the variation of subduction style along strike. Here we report results from a dense seismograph deployment carried out in the central North Island in 2001. This deployment (codenamed CNIPSE for Central North Island Passive Seismic Experiment) was concurrent with a number of other active and passive seismic experiments in the same region (Henrys *et al.* 2003a). We have combined CNIPSE data with that from the New Zealand national seismograph network, nearby previous dense seismograph deployments, large onshore shots and earthquake data recorded by a line of ocean bottom seismographs (OBSs) stretching from the east coast to beyond the Hikurangi Trench. This has allowed detailed 3-D modelling of both the *Vp* and *Vp*/*Vs* structure of the subduction zone, from the trench to 300 km depth.

The resulting tomographic images have provided insight into outstanding questions on the distribution of magmatism in the North Island. These include: (1) why does magmatism cease at the southwestern end of the TVZ, even though the subducted plate extends at least 350 km further to the southwest, and there has clearly been enough subduction in this region to expect magmatism and (2) why is the modern central TVZ the most frequently active and productive silicic volcanic system on Earth (Wilson *et al.* 1995)?

TECTONIC AND GEOLOGICAL SETTING

In the central North Island, the Pacific and Australian plates are converging obliquely at about 42 mm yr^{-1} (DeMets *et al.* 1994; Fig. 1). This convergence is accommodated by subduction of the Pacific plate and deformation of the overlying Australian plate. The general shape of the subducted plate has been revealed by compilations of seismicity located with the New Zealand national seismograph network (e.g. Anderson & Webb 1994). The dipping seismic zone associated with the subducted plate has a strike of 040° (Ansell & Bannister 1996), and extends to about 300 km depth beneath the western part of the region. Infrequent events also occur within a cluster of activity centred 600 km below Taranaki (Boddington *et al.* 2004).

At the east coast in Hawke Bay, the plate interface (as defined by the upper envelope of activity in the dipping seismic zone) is about 15 km deep, and dips to the northwest at 10°. The coastal region thus overlies the seismogenic zone of the plate interface, which may be capable of producing large subduction thrust earthquakes (e.g. Hyndman *et al.* 1997). Both seismological and GPS data suggest a southward increase in interseismic coupling at the seismogenic zone (Reyners 1998; Wallace *et al.* 2004). This results in much of the forearc rotating clockwise as several, distinct tectonic blocks, at rates of 1.6–3.8° Myr^{-1}. This rotation accommodates much of the margin-parallel component of motion between the Pacific and Australian plates (Wallace *et al.* 2004).

The rotation of the forearc has resulted in extension in the TVZ in the backarc continental crust of the northern part of the central North Island (Fig. 1). Both geodetic and fault slip data suggest an extension rate in the 4–10 mm yr^{-1} range (Darby & Meertens 1995; Villamor & Berryman 2001). Andesitic activity started in the TVZ *ca.* 2 Myr ago, joined by voluminous rhyolitic (plus minor basaltic and dacitic) activity from *ca.* 1.6 Myr ago. Volcanic activity within the TVZ changes character along strike, with rhyolite dominant caldera volcanoes in the central section and andesite dominant cone volcanoes to the north and south (Wilson *et al.* 1995; see Fig. 1). The modern central TVZ is the most frequently active and productive silicic volcanic system on Earth, erupting rhyolite at *ca.* 0.28 m^3 s^{-1}, and available information suggests this has been so for at least the past 0.34 Myr (Wilson *et al.* 1995). The average heat flux from the central 6000 km^2 of the TVZ is very high at 700 mW m^{-2} (Bibby *et al.* 1995).

Volcanism in the TVZ ends at the andesitic Mt Ruapehu (Fig. 1), and further south the backarc is characterized by compression. Dramatic subsidence in this region has formed the Wanganui Basin, which contains 5 km of Pliocene–Pleistocene shoreline–shelf marine sediments (Carter & Naish 1999). Multichannel seismic reflection data are interpreted to show that the reflection Moho has been flexed downward beneath the Wanganui Basin, and Stern *et al.* (1992) attribute the development of the basin to frictional shear between the subducted Pacific plate and overriding Australian plate. Andesitic volcanism does occur in this region at Mt Taranaki (Fig. 1), but this is about 130 km west of the volcanic front of the TVZ at Mt Ruapehu.

The basement geology of the central North Island consists of terranes which were accreted onto the Gondwana supercontinent in the Mesozoic, as described by Mortimer (2004). There is little basement exposure outside the axial ranges, where the greywacke Torlesse composite terrane is exposed. The axial ranges are actively uplifting regions of high relief, and include the Kaimanawa Mountains, the largest area of high relief in the North Island. The active North Island Dextral Fault Belt (Beanland 1995) cuts obliquely through the ranges (Fig. 1). East of the axial ranges, the Hikurangi forearc consists of mainly onshore forearc basins, including the Wairoa Syncline which contains up to 5 km of post-Cretaceous sediments (Field *et al.* 1997). These are separated from the mostly offshore accretionary prism (Lewis & Pettinga 1993) by the rapidly uplifting Coastal Ranges (Cashman *et al.* 1992).

DATA

CNIPSE involved the deployment of 74 portable digital seismographs in the central North Island for the period 2001 January 8 to June 27 (Fig. 2a). 32 of these were broad-band seismographs, and the scientific rationale for the placement of these is described by Reyners & Stuart (2002). During the experiment, over 4700 earthquakes were located within or close to the seismograph network. These extend down to 300 km depth, and provide an excellent snapshot of seismicity within the Hikurangi subduction zone.

Here we use *P* and *S* arrival times from a subset of the best-recorded events in a tomographic inversion for seismic velocity structure. For the inversion events, we supplement CNIPSE data with those recorded by nearby stations of the national seismograph network. For 81 of the events, we have added *P* and *S* picks from two OBSs in Lake Taupo, and seven OBSs west of longitude 178°E. These OBSs operated for one month in 2001 January/February (Henrys *et al.* 2003b), and have proved very useful for improving the resolution of deeper structure beneath the forearc. We have also incorporated *P* picks from nine 500 kg onshore explosions, detonated as part of the North Island GeopHysical Transect (NIGHT—Henrys *et al.* 2003b).

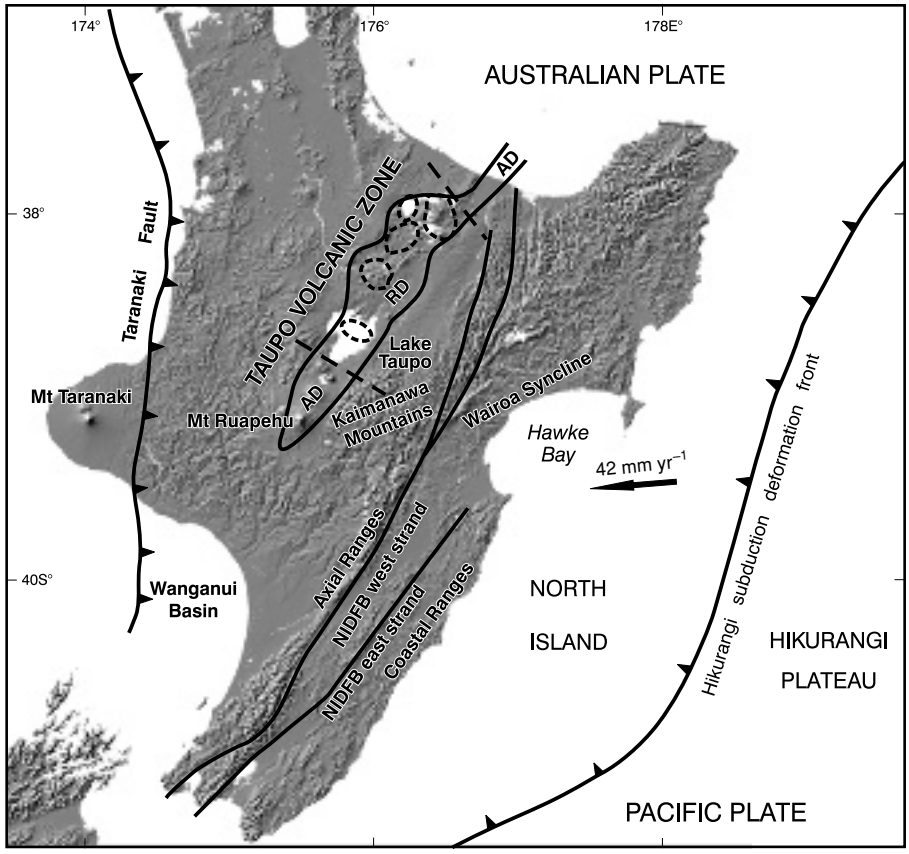

Figure 1. Topographic map of the central North Island and its tectonic setting. The arrow indicates the velocity of the Pacific plate relative to the Australian plate (DeMets *et al.* 1994). The TVZ is outlined and subdivided into three distinct segments—andesite dominant (AD) cone volcanoes in the northern and southern segments, and rhyolite-dominant (RD) caldera volcanoes (shown dashed) in the central segment (Wilson *et al.* 1995). NIDFB denotes the North Island Dextral Fault Belt.

The resulting inversion dataset still had uneven ray density in some areas, so we added more events, particularly at the edges of the CNIPSE network. We have included data from two PANDA (portable array for numerical data acquisition; Chiu *et al.* (1991) portable telemetered networks that were deployed along the southwest side of the study area in 1993 and 1994 (Fig. 2a). Accurate time corrections for the master clocks of both these telemetered networks are not available. So when combining PANDA data with data from the national seismograph network we solve for two earthquake origin times, as described by Eberhart-Phillips *et al.* (2005). We have also added data from larger intermediate depth events on the northwest edge of the study region occurring during the period 1990–2001, which were well recorded by the national seismograph network. The final inversion dataset includes 1239 earthquakes and nine explosions, and contains 39 123 *P* observations and 18 331 *S* observations. Arrival time picks were weighted by quality, with good *P* arrivals picked with an uncertainty of <0.03 s and good *S* arrivals with an uncertainty of <0.1 s.

METHOD

We use the arrival times of the earthquakes and shots in a simultaneous inversion for both hypocentres and the 3-D *Vp* and *Vp*/*Vs* structure (Thurber 1983, 1993; Eberhart-Phillips 1990, 1993; Eberhart-Phillips & Michael 1998). Our goal is to obtain a reasonable model for interpreting crust and mantle structure, for use in locating earthquakes and computing ray paths (azimuths and take-off angles) for focal mechanisms, and for including heterogeneous elastic moduli in deformation modelling. We would like to avoid a model with peculiar or unbelievable velocity anomalies, even if only in areas of low resolution, as such a model would be less straightforward to use for other purposes. We prefer to obtain *Vp* and *Vp*/*Vs* models rather than *Vp* and *Vs* models. *Vp*/*Vs* is an important parameter in characterizing rock properties and rheology. Particularly, in cases such as ours where *S* data are less numerous and of poorer quality than the *P* data, *Vs* would be poorly resolved compared to *Vp*, making the interpretation of *Vp*/*Vs* variations difficult (Eberhart-Phillips 1990). Solving for *Vp*/*Vs* makes the assumption that given a 3-D heterogeneous *Vp* model and unknown *Vs*, it would be better to estimate a *Vs* model from the *Vp* using a constant *Vp*/*Vs* than to assume a homogeneous *Vs* model.

The velocity of the medium is parametrized by assigning velocity values at the intersections (nodes) of a 3-D grid, with linear interpolation between nodes. The ray paths are calculated with an approximate 3-D ray-tracing algorithm that produces curved non-planar ray paths which are defined by points more finely spaced than the velocity nodes. This is a Cartesian grid with conversions done using the New Zealand Map Grid (Reilly 1973), and an earth-flattening transformation (Buland & Chapman 1983) for velocity during ray tracing. Actual station elevations were used for the ray tracing. The solution is obtained by iterative, damped least squares. Damping leads to a conservative solution that fits the data well with few artefacts. Thus selected damping parameters greatly reduce data variance with moderate increases in model variance (Eberhart-Phillips 1986). For each

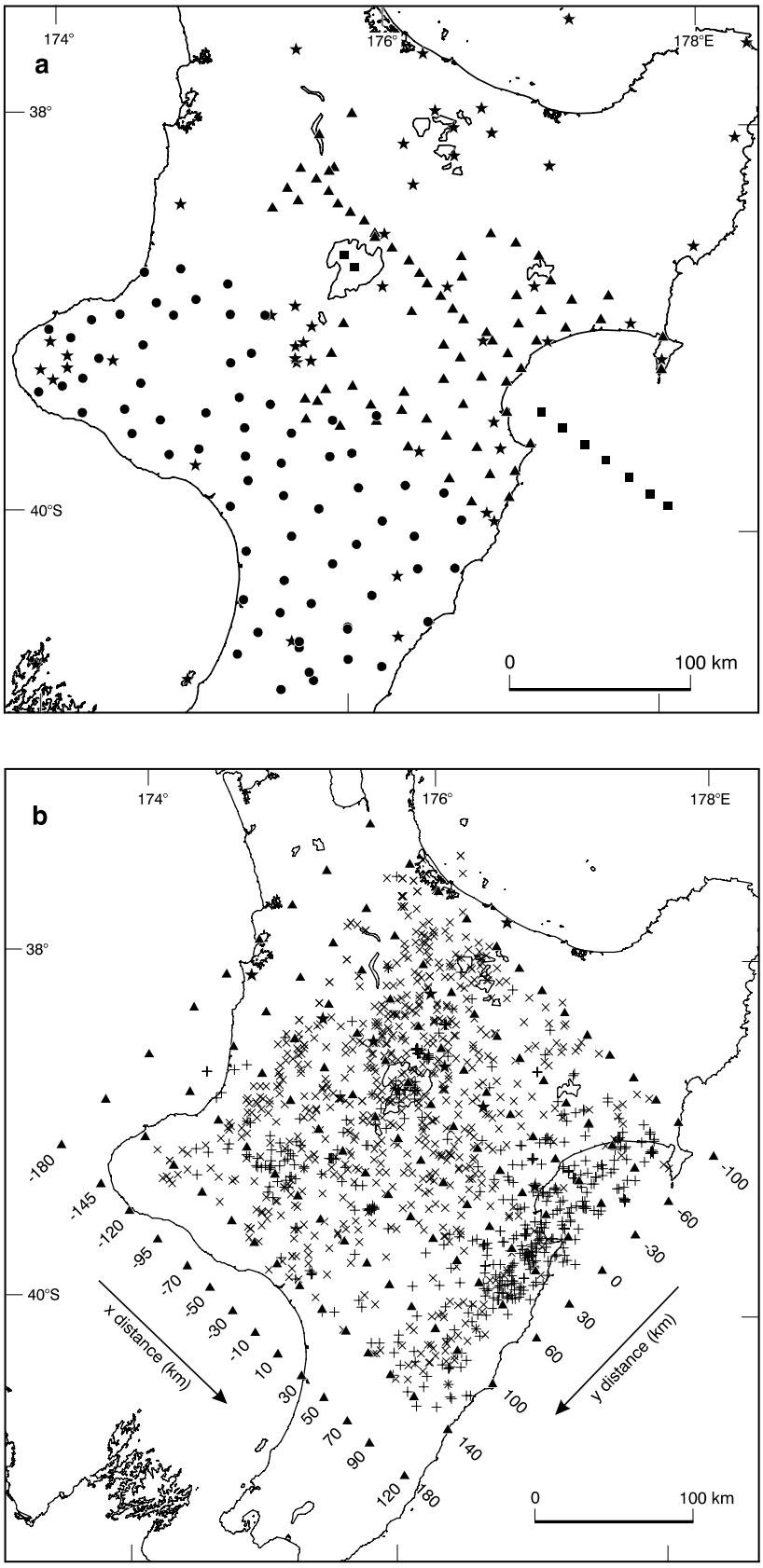

Figure 2. (a) Map of seismograph stations contributing data to the inversion. Stars are permanent stations of the New Zealand national seismograph network, triangles are portable CNIPSE stations, circles are portable PANDA stations, and squares are ocean bottom seismographs. (b) Map of earthquakes used in the inversion (pluses for events shallower than 40 km, crosses for deeper events), shots (stars) and the inversion nodes (triangles).

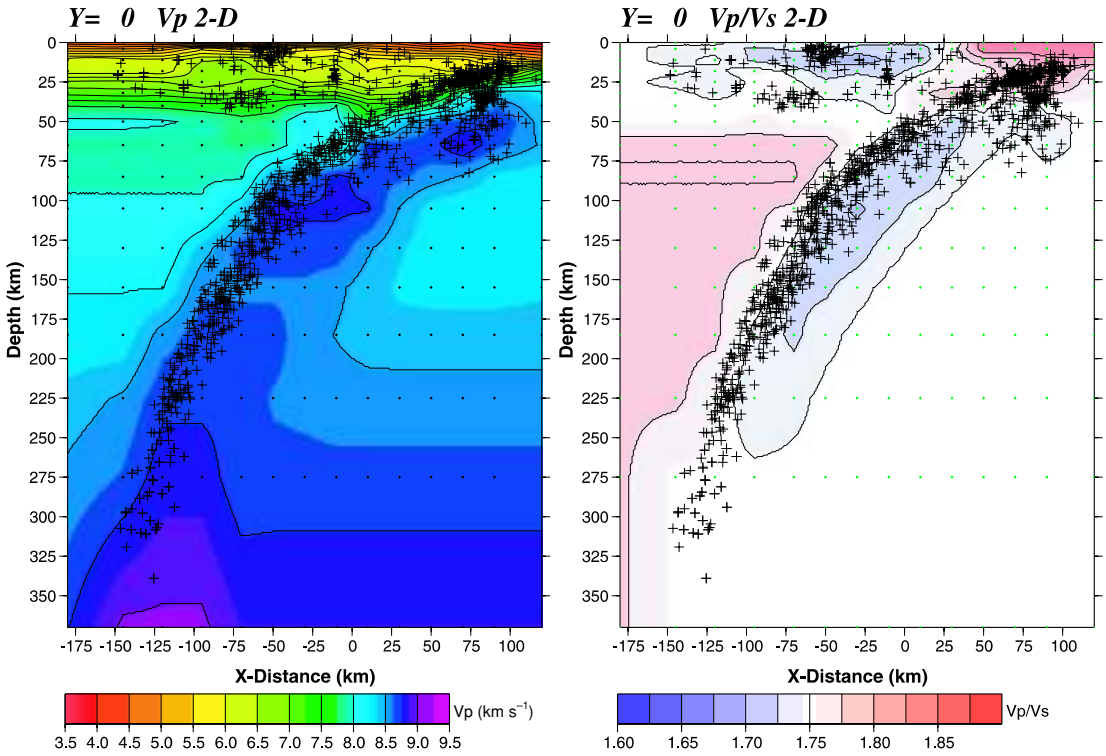

Figure 3. Depth sections down the dip of the subducted plate of the 2-D *Vp* (left) and *Vp/V*s (right) models showing inversion nodes (small dots) and relocated hypocentres of the inversion events (pluses).

iteration, new ray paths are determined, the hypocentre solution is included, and parameter separation is carried out. The full resolution matrix is also calculated. Throughout the inversion, weighting is applied to each observation, based on observation quality, source–receiver distance, and size of residual. Residuals greater than 0.75 s are greatly downweighted and residuals greater than 2.75 s are discarded since they are most likely erroneous readings (only 11 of the 57 454 observations were discarded). When the model velocities are not close to the actual velocities, high residuals may be more representative of velocity heterogeneity, and thus in the initial inversions, high downweighting was only applied for residuals greater than 1.75 s.

We performed a series of inversions of increasing complexity: 1-D, 2-D and 3-D. Such a series of progressive inversions will have a smooth regional model in places of low resolution. The initial crustal velocity model and initial hypocentres were obtained through simultaneous inversion for 1-D *Vp*, station corrections and hypocentres (Kissling *et al.* 1994). As deeper parts of the 1-D model were poorly resolved, velocities below 220 km were fixed to those of the preliminary reference earth model (Dziewonski & Anderson 1981). Even in the 1-D model, the gross features of the subduction zone are revealed by the station corrections. These range from −0.7 s in the southeast to +0.9 s in the northwest, suggesting fast paths up the subducted plate and slow paths through the uppermost mantle of the overlying plate.

The velocity grid used for both the 2-D and 3-D inversions is shown in Fig. 2(b). The coordinates were chosen to parallel the strike of the subduction zone in the region (040°). The *y*-axis is positive to the southwest and the *x*-axis is positive to the southeast. The distribution of *x*- and *y*-grid points was based on ray density. The same is true of *z*-grid points, which were fixed at 0, 4, 11, 18, 25, 32, 40, 50, 65, 85, 105, 130, 155, 185, 225, 275 and 370 km. There are only a few earthquakes deeper than 225 km so the deepest grids will generally retain the initial model. The regional structure is approximately 2-D along the *y*-axis, so a 2-D inversion for both *Vp* and Vp/Vs along $y = 0$ was done to obtain an initial model for the 3-D inversions. Linked nodes were used in the 2-D inversion to obtain both better resolution and a smooth model. Since the 2-D model is being used as the initial model for the 3-D inversions, it should be relatively smooth and not be dominated by small features that may not characterize the whole region. The resulting depth sections are shown Fig. 3. Even though we solve for seismic velocities at the nodes of a rectangular grid, the dipping subducted plate is clearly imaged by both *Vp* and Vp/Vs.

We then carried out a 3-D inversion using the nine y-grids, with station corrections allowed. Finally an additional 3-D inversion for only the $z = 0$ nodes was carried out without station corrections to improve the shallow velocities. The 3-D model achieved a 73 per cent reduction in traveltime data variance compared with the 1-D model.

Resolution of the final 3-D model is shown in Fig. 4 for the depth sections shown in Fig. 5. The resolution matrix describes the distribution of information for each node, such that each row is the averaging vector for a parameter. The relative size and pattern of the off-diagonal elements show the way the information is smeared. For a node to be adequately resolved, its resolution should be peaked and should have no significant contribution from nodes that are not adjacent. For a succinct way of assessing the resolution, we calculate the spread function (SF) (Michelini & McEvilly 1991; Michelini 1991), which describes how strong and peaked the resolution is for each node. We also illustrate the pattern of image blurring in low-resolution areas by showing contours of the averaging vectors for nodes that have significant smearing (Fig. 4). From each row of the resolution matrix we compute smearing contours where

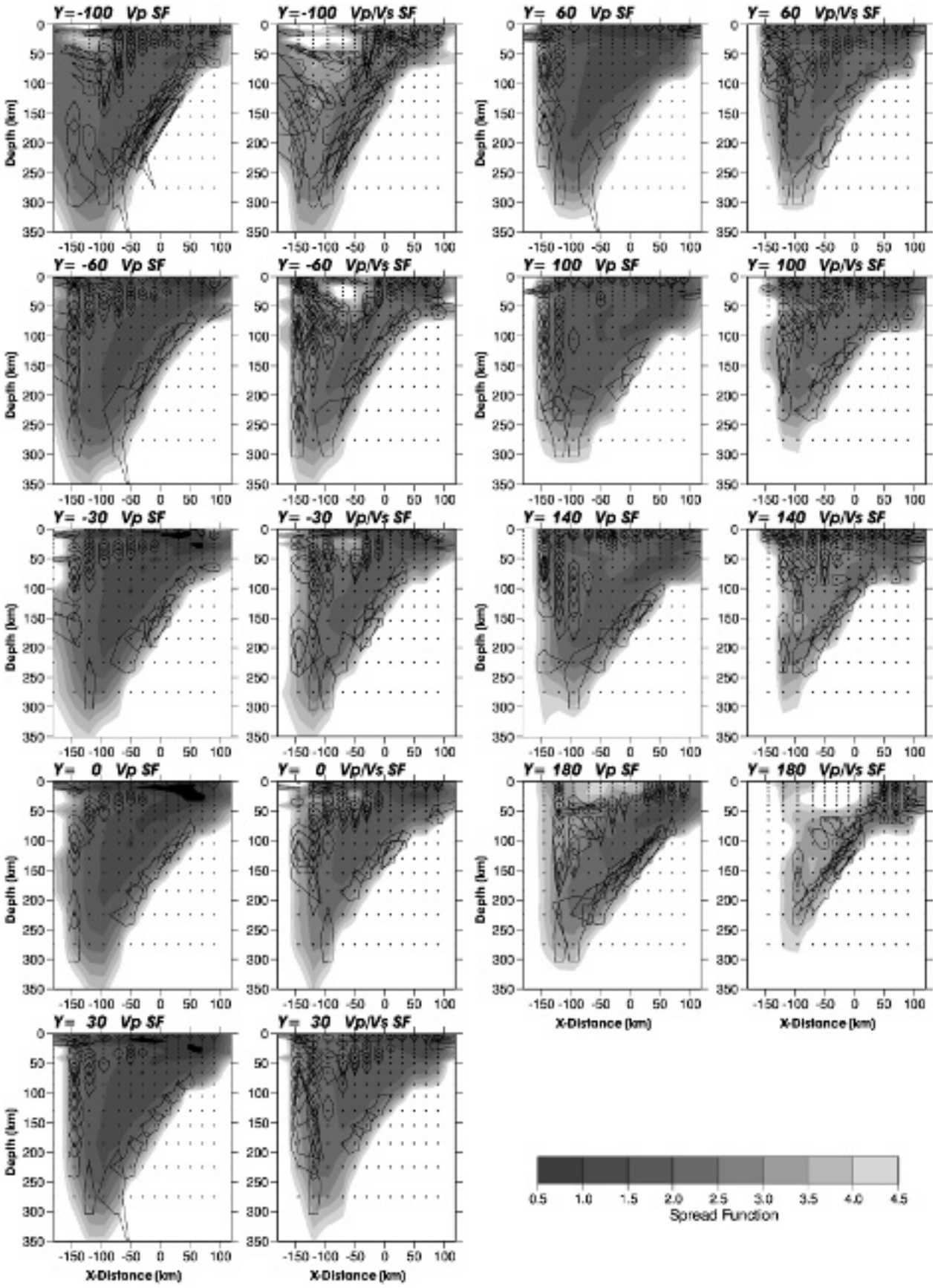

Figure 4. Resolution for *y* cross-sections of the 3-D *Vp* and *Vp/V*s models, showing the spread function and 70 per cent smearing contours for nodes that have significant smearing.

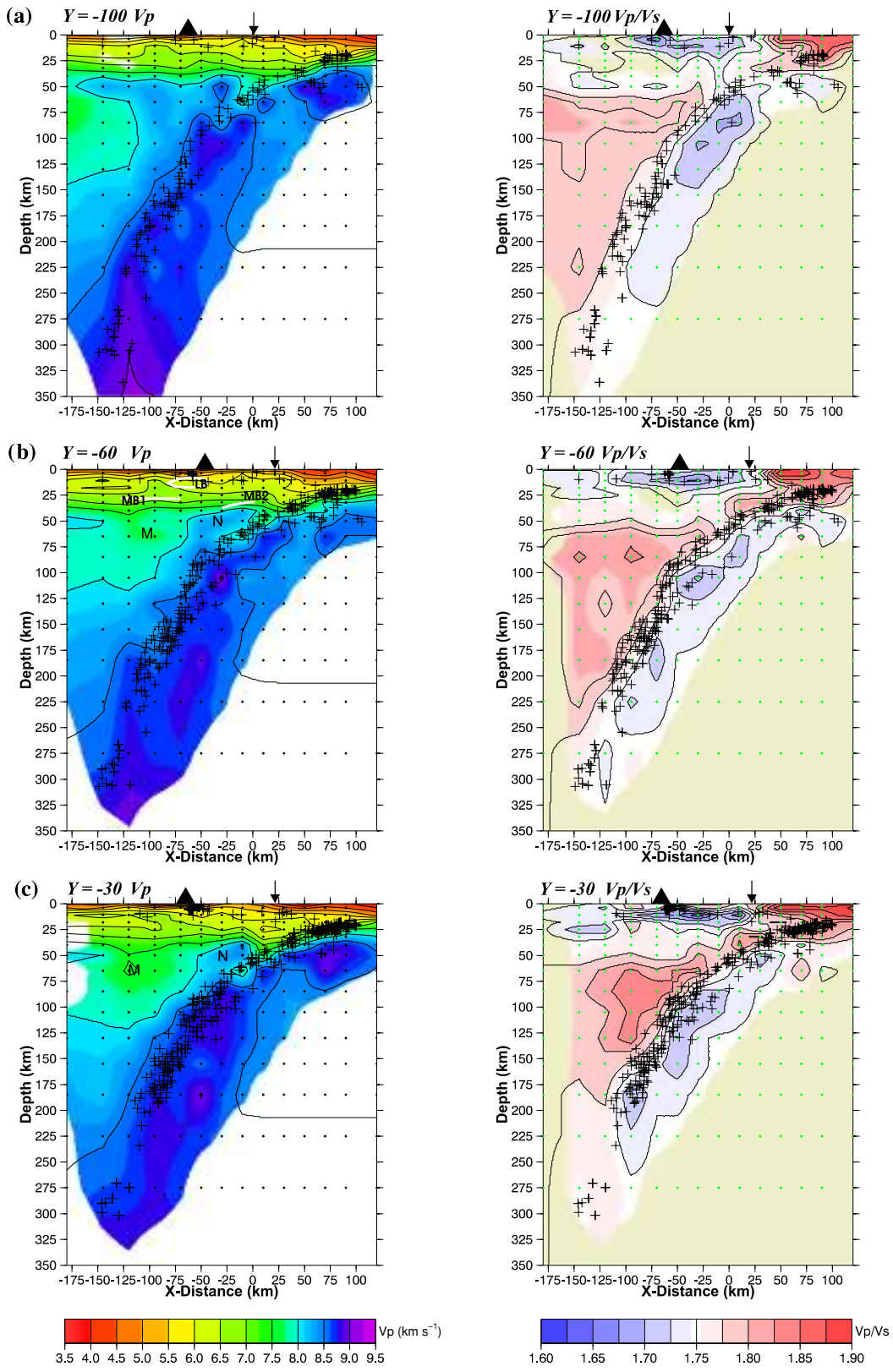

Figure 5. *y* cross-sections of the 3-D *Vp* (left) and *Vp/V*s (right) models. Regions with spread function >3.75 are masked but contoured. Small dots indicate the velocity nodes, and pluses denote relocated hypocentres of the inversion events out to adjoining sections. At the surface, triangles denote volcanoes and arrows indicate strands of the active North Island Dextral Fault Belt. On the *Vp* cross-sections in the mantle wedge, M denotes regions of partial melt and N denotes regions of stagnant mantle nose, interpreted from both *Vp* and *Vp*/*Vs*. On the *Vp* cross-section in (b), MB1 and MB2 indicate the Moho, and LB a crustal low-velocity zone, determined by Bannister *et al.* (2004) from receiver function inversion, while on the *Vp* cross-section in (d), MS1 is the top of a high *Vp* region and MS2 is a strong reflector identified by Stratford & Stern (2004) from active source data.

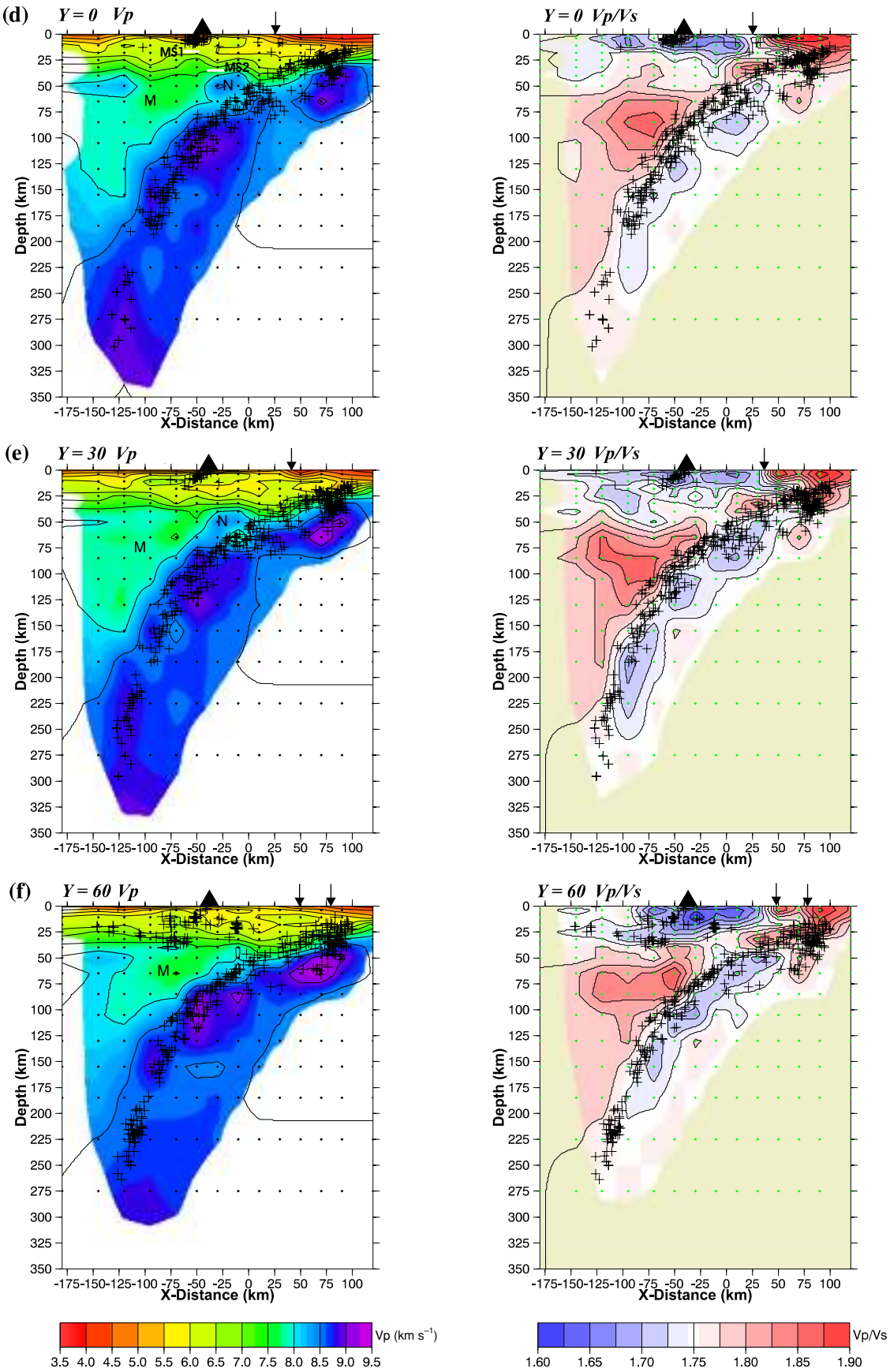

Figure 5. (*Continued.*)

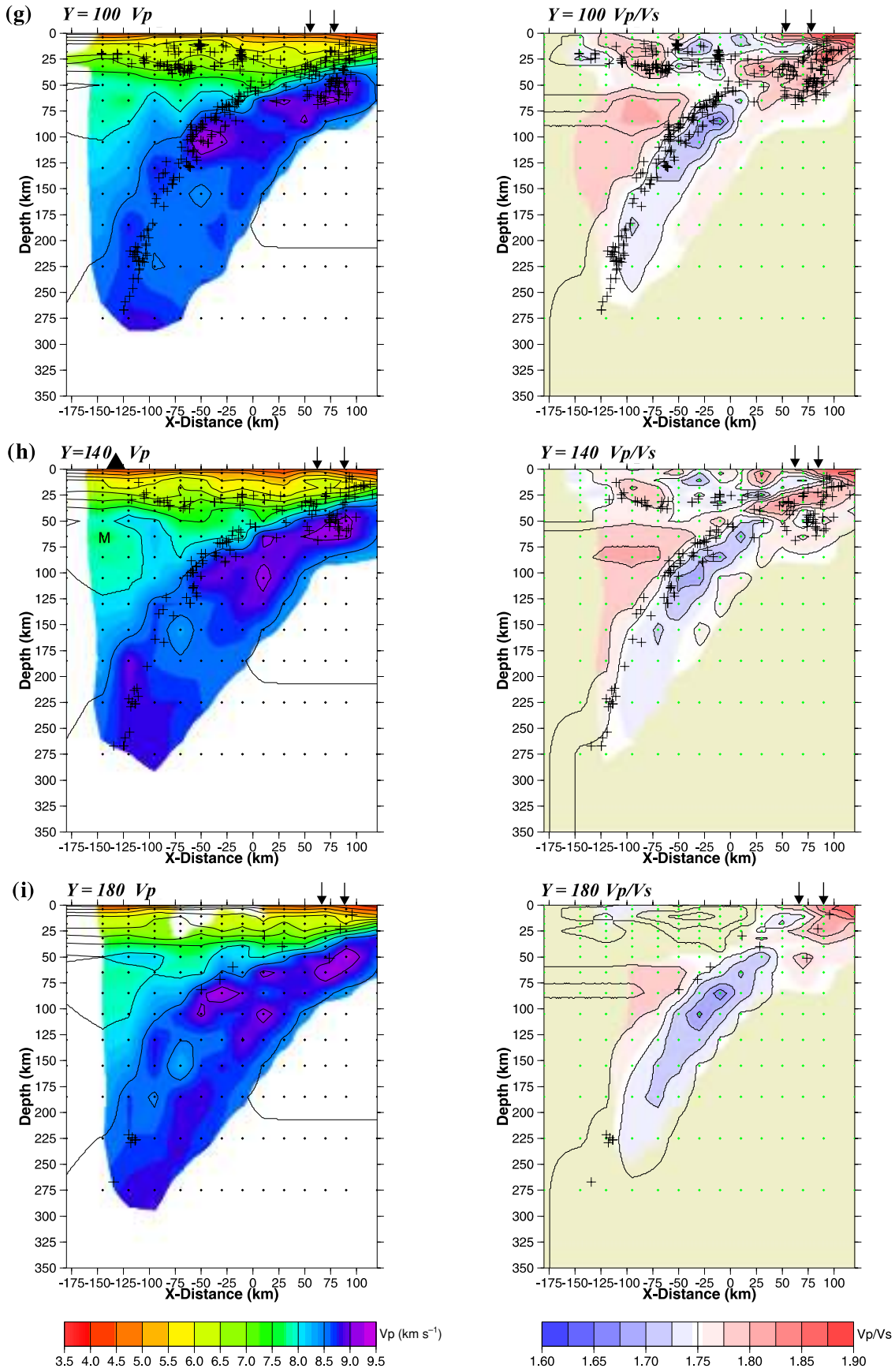

Figure 5. (*Continued.*)

the resolution is 70 per cent of the diagonal element (Reyners *et al.* 1999). Resolution contours are shown only for those nodes that have smearing such that the resolution contour extends beyond an adjacent node. At other nodes, we would expect the spatial averaging to be represented by the grid spacing.

The reliability of features in the 3-D inversion can be evaluated by combined use of the SF and resolution smearing contours. For low values of the SF (< 2.5) the model Vp or Vp/Vs is representative of the volume surrounding a given node—that is, the volume between that node and adjacent nodes. Nodes with moderate SF values ($2.5 < \mathrm{SF} < 3$) have acceptable resolution, but may be averaging a larger volume, and small features may not be imaged or may appear as broad features. Nodes with SF values in the 3–3.75 range have meaningful velocity patterns, but the size of the velocity perturbations may be smaller than actual velocity heterogeneity. Higher SF values indicate little or no information, and the associated Vp or Vp/Vs remains close to the initial model.

In the discussion which follows, we define regions of high or low Vp relative to the average Vp at the same depth. Similarly, we define regions of high or low Vp/Vs relative to the average Vp/Vs of the complete dataset of 1.75, determined from a Wadati diagram.

DISCUSSION OF RESULTS

Subducted plate

The subducted plate is clearly imaged as a high Vp, low Vp/Vs feature in both the 2-D and 3-D inversions (Figs 3 and 5). At depths less than 50 km, the upper band of seismicity in the dipping seismic zone parallels the velocity contours, and lies in a region with Vp in the 7.0–7.5 km s^{-1} range. This is consistent with these earthquakes occurring in the mafic crust of the subducted plate. At greater depths, the dipping seismic zone tends to dip more steeply than the Vp contours, suggesting a migration of seismicity into the high-velocity core of the subducted slab (e.g. Fig. 5e). This contrasts with the Vp/Vs contours, which closely parallel the dipping seismic zone down to at least 250 km, where resolution becomes poor.

The dipping seismic zone has a rather simple shape, with the upper envelope of the relocated events closely approximating a circular arc of *ca.* 300 km radius. Below 200 km the dipping seismic zone is close to vertical (e.g. Figs 5e–g). The deepest events in Taranaki (Fig. 5h) directly overly the 600-km-deep events relocated by Boddington *et al.* (2004), suggesting the possibility of a continuous vertical slab to this depth. The dipping seismic zone does not show any pronounced downdip bends, as suggested by Reyners (1980). Also, there is no pronounced thickening of the dipping seismic zone in the 120–220-km-depth range, as shown by the seismicity compilation of Anderson & Webb (1994). Both these features are artefacts resulting from the 1-D velocity models used in these previous studies. This emphasizes the importance of using 3-D velocity models for routine location of earthquakes in the central North Island.

Many of the depth sections show evidence of a double seismic zone (e.g. Figs 5b–d), with the lower plane converging with the upper plane at 130–140 km depth. Earthquakes in the lower plane generally occur within or close to regions of the slab mantle where Vp is relatively high. There appears to be significant variation in the productivity of earthquakes in the lower plane along the strike of the subduction zone (Fig. 5). The lower plane is also associated with a region of relatively low Vp/Vs. This feature is similar to the low Vp/Vs in the vicinity of lower plane earthquakes in the northern Honshu (Japan) subduction zone revealed by double-difference tomography (Zhang *et al.* 2004). Earthquakes in the lower plane are likely to be promoted by dehydration embrittlement of serpentinized mantle (Hacker *et al.* 2003b; Yamasaki & Seno 2003). Under the pressure and temperature conditions expected at ~100 km depth, serpentine will start to transform into forsterite and enstatite plus ~13 wt per cent water (Ulmer & Trommsdorff 1995). Serpentine has an unusually high Vp/Vs of *ca.* 2.11 (Christensen 1996). In contrast, laboratory studies show that a forsterite–enstatite composite with a forsterite volume fraction of 0.6 has $Vp \sim 8.5$ km s^{-1} and $Vp/Vs \sim 1.71$ at 2.5 GPa pressure (Ji & Wang 1999). These Vp and Vp/Vs values are similar to what we observe in the region of the lower plane, suggesting that here serpentinite has largely dehydrated and we are imaging a forsterite–enstatite–water system.

The Vp resolution within the subducted slab is adequate to 225 km depth on most sections (Fig. 4), and hence the heterogeneity in the slab represents real velocity variations tracking changes in mineralogy with depth. Vp within the subducted slab mantle is almost always >8.5 km s^{-1}, and is locally >9.0 km s^{-1}. The highest velocities may be there to produce sharp gradients in the coarsely parametrized model. Below the forearc these velocities replicate high velocities obtained previously from earthquake studies and seismic refraction experiments (Galea 1992; Chadwick 1997). Vp appears to be highest to the southwest of Lake Taupo, in concert with lower Vp/Vs (Figs 6i–k). These velocities are higher than those usually seen in the mantle of a subducted plate (e.g. Nakajima *et al.* 2001a). They require the slab, which is *ca.* 120 Myr old (Hoernle *et al.* 2004), to be unusually cold (Hacker *et al.* 2003a).

Can we identify the subducted Hikurangi Plateau in our tomographic images, given that the crust of the plateau is about 17 km thick to the east of the central North Island (Davy & Wood 1994)? Thick subducted crust has been imaged with local earthquake tomography in other regions (e.g. Eberhart-Phillips *et al.* 2003). On the depth sections shown in Fig. 5, we can identify a region with $Vp < 8.0$ km s^{-1}, which extends discontinuously from the base of the Australian plate crust to *ca.* 65 km depth, and is surrounded above and below by higher velocity mantle. This feature is continuous along strike in the region where resolution is good (see region denoted by H in Figs 6f–i). As this dipping lower-velocity zone coincides with the upper part of the dipping seismic zone, we can relate it to subducted crust of the Hikurangi Plateau. Both the Vp and Vp/Vs of the zone are similar to those in the subducted crust further updip.

Two explanations are possible for the rather abrupt termination of the low-velocity zone at *ca.* 65 km depth. The first is that this marks the transformation of the metabasalt and metagabbro of the crust of the subducted plateau to eclogite (Kirby *et al.* 1996). There are problems with this interpretation. Firstly, if the slab is as cold as the Vp in the slab mantle suggests, this transformation should be rather gradual and not be complete until much deeper. For example, for the cold 130 Myr old subducted Pacific plate in northeast Japan, thermal and petrological modelling suggests this transformation is not complete until 150 km depth (Hacker *et al.* 2003b). Also, the plateau has about twice the thickness of normal oceanic crust, and thus will have approximately four times the thermal time constant (Kirby *et al.* 1996). This should delay eclogite formation to still greater depth. Furthermore, we do not see a decrease in seismicity in the dipping seismic zone below 65 km depth, which we would expect if these events are due to dehydration embrittlement and are thus inhibited in anhydrous eclogite. Our preferred explanation is that ~65 km depth marks the leading edge of the subducted Hikurangi Plateau, and downdip from this is oceanic crust of normal thickness, which is not well imaged by our velocity grid. Little direct evidence

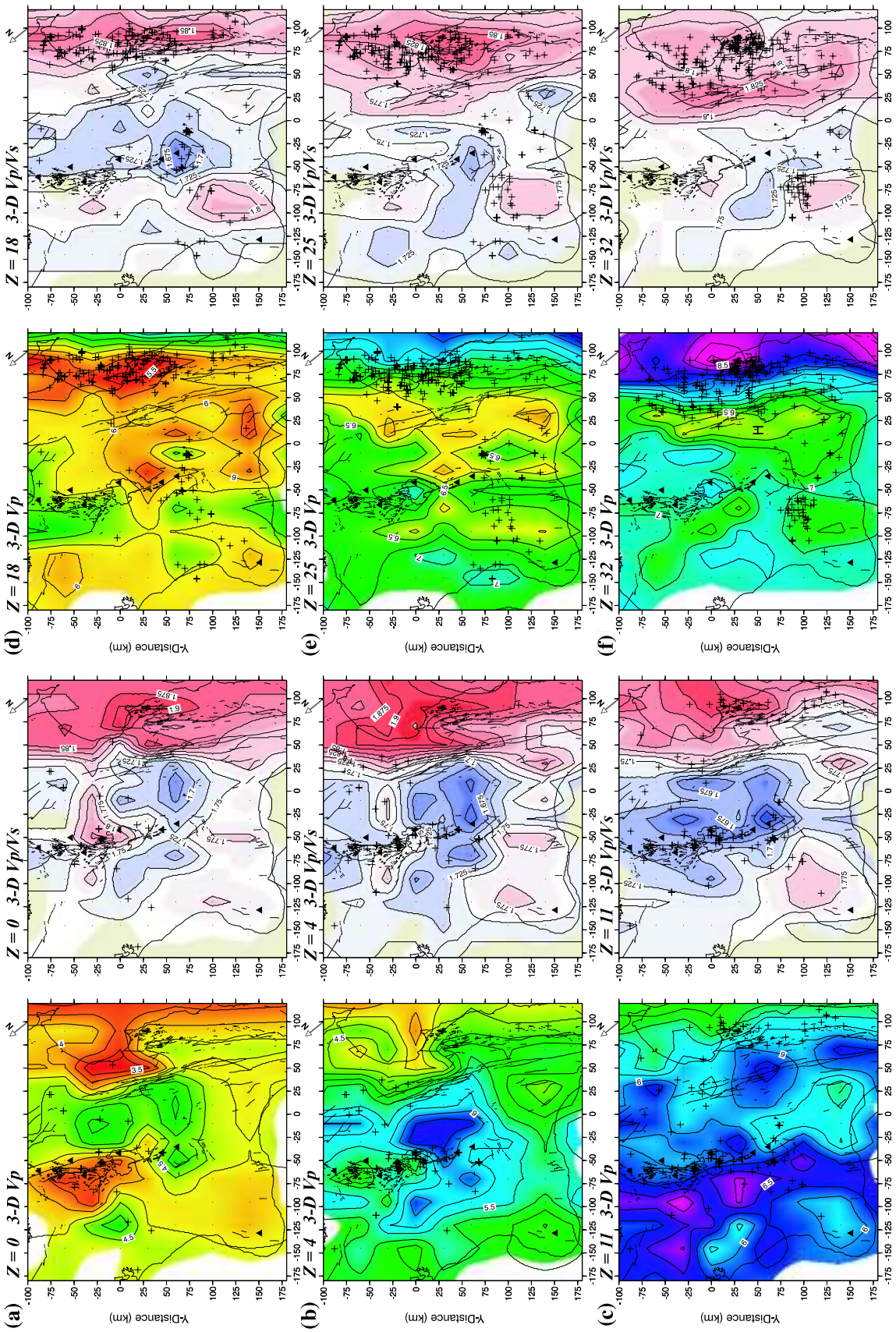

Figure 6. Map views of the 3-D *Vp* and *Vp/Vs* models. *Vp* is contoured at 0.25 km s^{-1} and *Vp/Vs* at 0.025. The *Vp* colour scale changes for each column (after every third depth slice), while the *Vp/Vs* colour scale is common to all depths. Small dots indicate the velocity nodes, and pluses denote relocated hypocentres of the inversion events out to adjoining depth slices. Thin lines denote active fault traces, and triangles are volcanoes. On the *Vp* maps, regions in (f)–(i) denoted by H are interpreted as thick subducted crust of the Hikurangi Plateau, regions in (i)–(l) denoted by M are interpreted as partial melt in the mantle wedge, and the region in (g) denoted by C is interpreted as thick backarc crust.

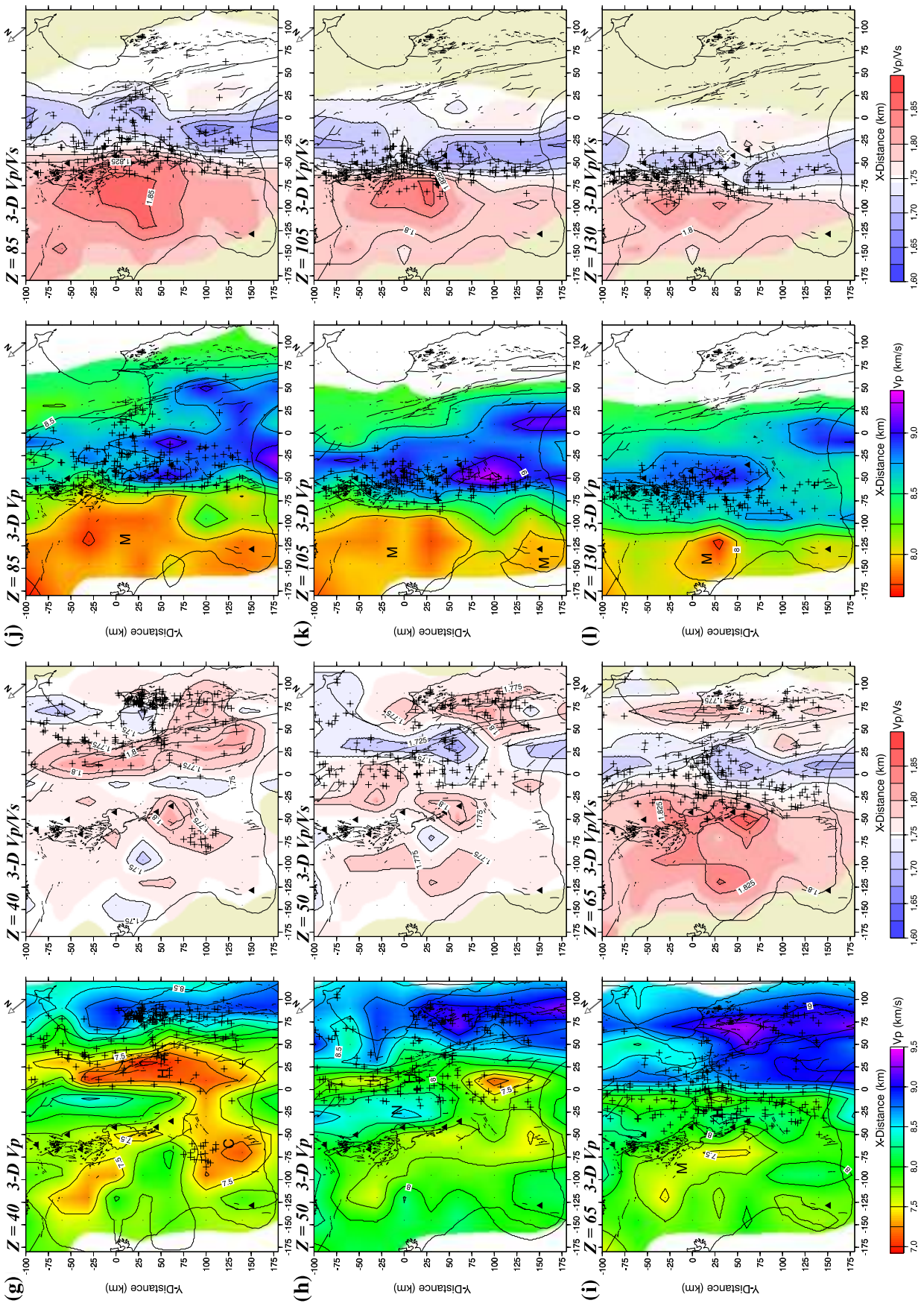

Figure 6. (*Continued.*)

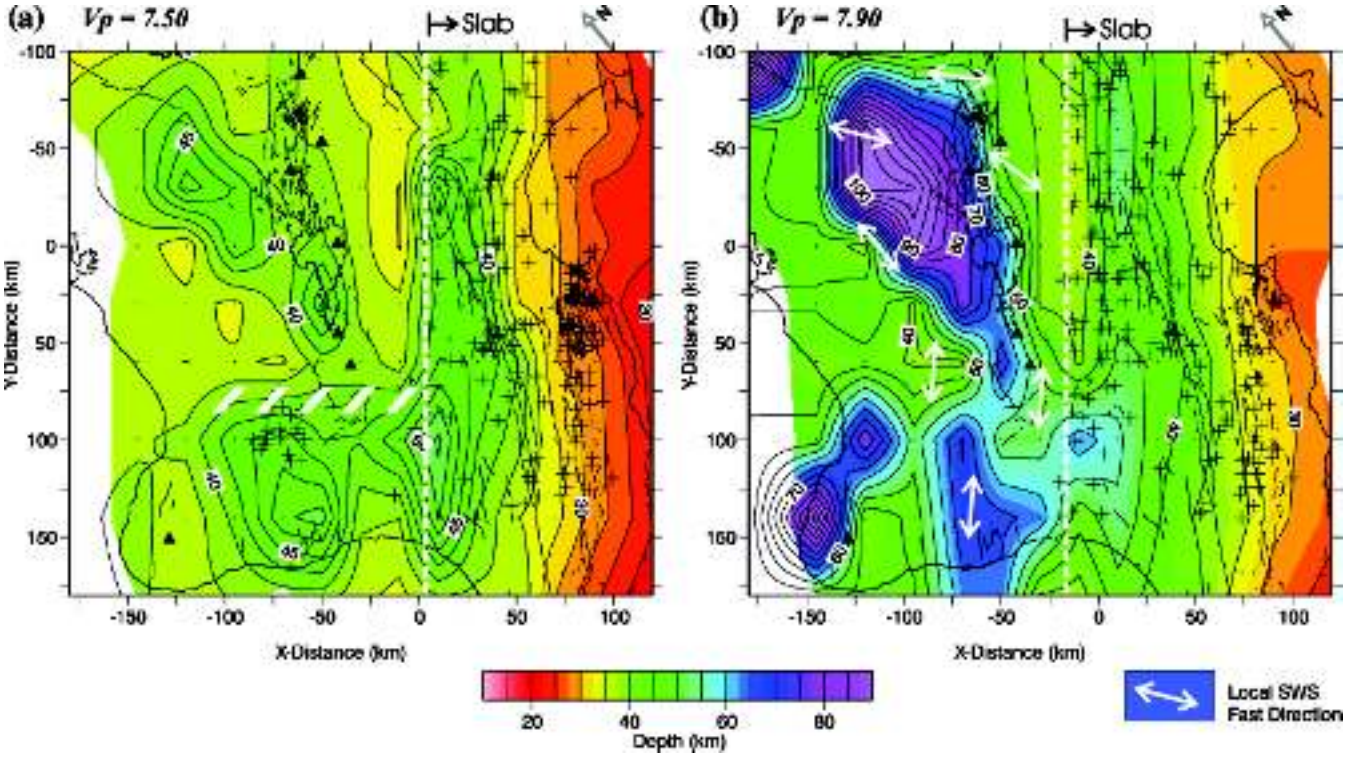

Figure 7. Depth variation of the isovelocity surface for $Vp = 7.5$ km s^{-1} (a) and $Vp = 7.9$ km s^{-1} (b). Depth contours are at 2.5 km intervals. The dashed line in both figures separates structure within the subducted slab to the southeast from that in the backarc and mantle wedge to the northwest. The hatched zone in (a) defines the region where the backarc crust thickens significantly to the southwest, and the arrows in (b) show spatially averaged fast shear wave splitting directions determined by Audoine *et al.* (2004).

of the history of Hikurangi Plateau subduction exists, except for slumping and subsidence in the wake of the northern edge of the plateau, as it sweeps along the Kermadec Trench some 500 km northeast of the central North Island (Davy & Collot 2000). If the low-velocity zone is diagnostic of the Hikurangi Plateau, it will have entered the subduction zone approximately 7 Ma ago. This timing is consistent with accelerated contractional deformation in the forearc during the period *ca.* 8.0–6.0 Ma (Nicol *et al.* 2002).

Mantle wedge

The mantle wedge is generally imaged as a low Vp, high Vp/Vs feature (Fig. 5). However, there are significant changes evident in the wedge along the strike of the subduction zone. The region where Vp is less than 8.0 km s^{-1} extends deepest northwest of the Lake Taupo region (Figs 5c–f, 6i–l, 7b). The lowest Vp in this region occurs at 65 km depth, locally reaching 7.4 km s^{-1}. This region also exhibits high Vp/Vs, which reaches 1.87 at 65 km depth. The high Vp/Vs region is clearly restricted along strike (Fig. 6j), as resolution is good in that direction. However, its northwestern extent is not as well controlled as resolution is poor beyond $x = -145$ (Fig. 4).

In the mantle wedge, the effects of water, high temperatures, and partial melt can all substantially reduce seismic velocity, and these effects are difficult to distinguish using seismic velocity measurements alone (e.g. Wiens & Smith 2003; Karato 2003). The spatial variation of temperature in the mantle wedge can be constrained by seismic attenuation data, since the presence of partial melt has little effect on seismic attenuation (e.g. Sato *et al.* 1989). A coarse 2-D attenuation model for the mantle wedge in the central North Island has been determined by Eberhart-Phillips & McVerry (2003), using local earthquake t^* data. This shows very low Qp of 100–200 within the wedge. Nakajima & Hasegawa (2003) have used similar attenuation data from the well-studied northeast Japan subduction zone to estimate the thermal structure of the mantle wedge. Their results suggest that a Qp of 100–200 indicates a temperature higher than the wet solidus of peridotite. We thus interpret the low Vp region within the mantle wedge as a region of significant partial melt, produced by the reaction of fluid released by dehydration of the subducted plate with the convecting mantle wedge (e.g. Tatsumi 1989). This region is identified by M in Figs 5 and 6.

It is noteworthy that the highest Vp/Vs region abuts the upper surface of the dipping seismic zone in the 85–105-km-depth range (Figs 6j and k). The b-value of the earthquake frequency magnitude distribution is anomalously high in this depth range, which has been interpreted as indicating high pore pressures in the top of the subducting plate (Wiemer & Benoit 1996). In contrast, the region with lowest Vp, while paralleling the underlying dipping seismic zone, is located about 30 km from the upper surface of the zone (Figs 5d–f). This result is very similar to that of Eberle *et al.* (2002), who numerically model the thermal structure and flow-field of a subduction zone with a fixed upper plate and strongly temperature-dependent viscosity. Material in the $Vp > 8.0$ km s^{-1} region directly above the dipping seismic zone can be interpreted as sinking, entrained with the motion of the subducted slab, while material in the overlying low Vp region can be interpreted as rising within a return flow within the mantle wedge. The material dragged downwards forms a viscous blanket that insulates the slab from the high-temperature mantle wedge (Kincaid & Sacks 1997).

The dipping, low Vp region meets the base of the crust close to the volcanic front in the Taupo region (Fig. 6g). This situation is

similar to that determined for the northeast Japan subduction zone, where the location of the volcanic front appears to be controlled by where the upwelling mantle flow meets the Moho (Hasegawa & Nakajima 2004). Immediately southeast of the low *Vp* region there is a relatively high *Vp* region, located between the base of the crust and the dipping seismic zone (see region marked N in Figs 5b–e, 6h). This region can be interpreted as a stagnant mantle nose, where mantle flow is minimal (e.g. Eberle *et al.* 2002).

The significant along-strike variation of the low *Vp* and high *Vp*/*Vs* regions in the mantle wedge (e.g. Fig. 6i) suggests a variation of partial melt which is consistent with changes in volcanism seen at the surface. The lowest value of *Vp* we measure is at the node $x = -70, y = 30, z = 65$ (Figs 5e and 6i), where $Vp = 7.4$ km s^{-1}. This point lies just to the west of the active Taupo caldera. We can estimate the amount of partial melt at this point by determining values of $d\ \ln Vs / d\ \ln Vp$ (the velocity decrease ratio between *P* and *S* waves), using the methodology of Takei (2002). This ratio is estimated to be ∼1.3, consistent with the presence of texturally equilibrated partial melt.

The *Vp* and *Vp*/*Vs* anomalies become more subdued 50 km northeast of Lake Taupo ($y = -60$; Fig. 5b). This region lies near the northeastern limit of the productive, rhyolite-dominated central segment of the TVZ—to the northeast the zone narrows appreciably and becomes andesite dominated (Wilson *et al.* 1995). We cannot track this subdued anomaly further northeast as resolution becomes poor at the edge of our grid, especially for *Vp*/*Vs* (Fig. 4). To the southwest, the upper mantle anomaly ends abruptly between $y = 60$ and $y = 100$ (Fig. 6i). On the two southwest sections where resolution is good (Figs 5g and h), there is no significant low *Vp* zone in the mantle wedge paralleling the subducted plate, as is seen further northeast. The lowest *Vp* region lies much further northwest, particularly at 65 km depth near the andesitic Mt Taranaki volcano (see region marked M in Fig. 5h). This situation suggests that there is little return flow in the shallow part of the mantle wedge southeast of Mt Taranaki. A possible reason for this is the thicker than normal crust of the overlying plate in this region (see region marked C in Fig. 6g). Kincaid & Sacks (1997) have shown that thick upper plates choke off return flow, causing the cool, high-viscosity nose between the plates to advance into the wedge. Additionally, the compression seen in the crust in this region results in movement of the overlying plate towards the subducted plate, which will also suppress return flow (Eberle *et al.* 2002).

The low *Vp* region centred just northwest of the Lake Taupo region (labelled M in Fig. 6i) is a good candidate for the low density in the mantle wedge required to explain exhumation and landscape evolution in the central North Island in the last 5 Myr. Pulford & Stern (2004) use mudstone porosity analyses to demonstrate that a maximum of 2.5 km of rock uplift has occurred in this time. The centre of this uplift, where rates are locally >0.6 mm a^{-1}, corresponds closely with the low *Vp* region of this study. Pulford & Stern (2004) also interpret the zone of maximum incision erosion as indicating a southward migration of the locus of maximum rock uplift with time. This requires that the low *Vp*, high *Vp*/*Vs* region in the mantle wedge identified here also moves south.

Backarc crust

The 3-D model does not include discontinuities and the vertical node spacing is 7–10 km, so we can only estimate the base of the crust from the velocity gradients. The estimate of crustal thickness will be most accurate where there are earthquake sources throughout the crust, as occurs southwest of Mt Ruapehu (Figs 5f–h). To the northeast, where there are primarily upper crustal and slab earthquakes, there will be significant vertical smearing so that the velocity solution is effectively averaging over a greater depth extent than the vertical node spacing. Such vertical smearing is observed in the $y = -30$ cross-section (Fig. 4) and may influence the extent of the low *Vp* centred at $x = -120, z = 65$ (Fig. 5c). This feature could potentially have a more pronounced upper edge and be limited to below 40 km depth. In contrast, the low *Vp* in the southern TVZ centred at $x = -70, z = 65$ (Fig. 5e) is better resolved with less vertical smearing.

Northeast of Mt Ruapehu, the thickness of the backarc crust (as approximated by the $Vp = 7.5$ km s^{-1} contour) is close to that of normal continental crust, averaging *ca.* 35 km (Figs 5a–f). This result is consistent with previous estimates of crustal thickness immediately north of Lake Taupo, determined with both earthquake and explosive sources (Robinson *et al.* 1981; Harrison & White 2004). Structures inferred from receiver function and active source studies are shown in Figs 5(b) and (d). The eastern TVZ Moho inferred by Bannister *et al.* (2004), labelled MB2, is equivalent to a strong reflector identified by Stratford & Stern (2004), labelled MS2. Both these structures occur where there is a strong gradient in *Vp* in our model, consistent with this region marking the base of the crust. Underlying Lake Taupo, there is a distinctive localized region of high velocity in the lower crust, with *Vp* 7.2–7.5 km s^{-1} at 20–35 km depth (Fig. 5d, $x = -50$). The refraction model of Stratford & Stern (2004) places the top of this high *Vp* region at 16 km depth, labelled MS1 in Fig. 5(d). Our 3-D model shows that this high *Vp* region is spatially limited to the Lake Taupo area and does not extend further northeast or southwest (Fig. 6e). This is consistent with the receiver function results of Bannister *et al.* (2004) 50 km northeast of Lake Taupo, which do not show high *Vp* material at 20 km depth. The high *Vp* in the lower crust beneath Lake Taupo may represent heavily intruded and underplated crust, resulting from a large flux of magma in this region.

Southwest of Mt Ruapehu, the crust thickens to over 40 km (see region labelled C in Fig. 6g). The northeastern and northwestern boundaries of this thick crust are well resolved, but we cannot determine how far southwest it extends as resolution becomes poor beyond $y = 140$. The change in crustal thickness is well illustrated by a 7.5 km s^{-1} iso-velocity plot (Fig. 7a), which shows the depth at which 7.5 km s^{-1} is obtained in the 3-D model, and hypocentres near that depth. The right-hand side of this plot shows the dipping subducted plate. The left-hand side shows structure within the overlying plate—low *Vp* mantle and Taupo intrusives in the northeast, and a *ca.* 10 km increase in crustal thickness across the hatched zone to the southwest.

The northeastern edge of this thicker crust has previously been recognized as a major crustal boundary, based on the steep gravity gradient across it (Stern *et al.* 1987), changes in seismic attenuation and resistivity across it (Salmon *et al.* 2003), and a concentration of earthquakes in the lower crust near the boundary (Sherburn & White 2005). The *Vp* contours of the 3-D model (Figs 6g and 7a) suggest that this boundary trends southeast–northwest, parallel to the dip of the subduction zone. Seismicity in the lower crust is mostly located southwest of the boundary. It concentrates where *Vp* is *ca.* 7.0 km s^{-1} (Fig. 5g), suggesting that the lower crust is of mafic composition. This lower crust is also reflective (Stern & Davey 1989). The northwestern boundary of the thick crust (Figs 6f–g) is closely aligned with the Taranaki Fault (Fig. 1). This is a crustal scale thrust fault that has accommodated at least 12–15 km of dip-slip displacement in the last *ca.* 80 Myr (Nicol *et al.* 2004).

Because of the relatively coarse grid spacing in our inversion, we cannot distinguish fine features within the upper crust, such as shallow *Vp* anomalies associated with individual calderas (e.g. Sherburn *et al.* 2003). Nevertheless, our 3-D model is consistent with previous studies. Where Sherburn *et al.* (2003) image a zone of several 10 km wide near surface features with $Vp < 3$ km s^{-1} in the central TVZ, we image a 40-km-wide zone with $Vp < 3.75$ km s^{-1} (centred near $x = -75, y = -40$ in Fig. 6a). With receiver functions, which are capable of showing velocity reversals, Bannister *et al.* (2004) have delineated a crustal low-velocity zone from 8–16 km depth (labelled LB in Fig. 5b). Since this is below the crustal earthquake sources, our results only show a broad region of relatively low velocity without a velocity reversal.

Large rhyolitic eruptions, such as the Oruanui eruption 26.5 kyr ago which erupted *ca.* 530 km^3 of magma from the Taupo caldera (Wilson *et al.* 2006) require the development of significant bodies of melt in the mid and upper crust. The only extensive low-velocity zone within the crust where the 3-D model resolution is good occurs at *ca.* 18 km depth near the south end of Lake Taupo (centred near $x = -30, y = 30$ in Fig. 6d). Using the methodology of Takei (2002), we estimate that the value of $d \ln Vs / d \ln Vp$ for the grid point (−30, 30, 18) within this low-velocity zone is ∼1.0, consistent with the presence of texturally equilibrated partial melt. Such evidence for significant partial melt in both the crust and in the upper mantle (see earlier) suggests that the Taupo caldera is currently the locus of most active rhyolitic volcanism within the TVZ.

The rhyolite-dominated section of the TVZ, from Lake Taupo to the northeastern edge of our grid (Figs 5a–e) exhibits low *Vp*/*Vs* in the upper crust (<18 km depth). Similar low *Vp*/*Vs* has been observed beneath active volcanoes in northeastern Japan, and it can be explained by the presence of water (e.g. Nakajima *et al.* 2001a,b). The extensional stress regime of the TVZ ensures high bulk permeability in the crust, and hydrostatic fluid pressure conditions (Sibson & Rowland 2003). This region exhibits vigorous geothermal activity, which is known to be associated with low *Vp*/*Vs* (Chatterjee *et al.* 1985). The wide extent of the low *Vp*/*Vs* in this part of the TVZ (e.g. Fig. 6c) implies that there are no extensive regions of partial melt in the upper crust, at least with a volume larger than the spatial resolution of our inversion. In the lower crust, *Vp*/*Vs* increases rapidly. This is most likely due to the presence of regions of partial melt in the lower crust (such as that identified near the south end of Lake Taupo), and the accompanying magma overpressure.

In contrast, in the andesite-dominated southwestern section of the TVZ the low *Vp*/*Vs* extends into the lower crust (Fig. 5f). There is a particularly low *Vp*/*Vs* anomaly centred beneath Mt Ruapehu volcano ($x = -30, y = 65$; see Figs 6c–e). At the base of the crust (*ca.* 40 km) there is a very strong gradient to high *Vp*/*Vs* in the upper mantle, which can be related to an extensive region of partial melt (Fig. 5f). Thus the deep magma plumbing of this section of the TVZ is quite different to the rhyolite-dominated section further northeast. There appears to be no significant intrusion of magma into the crust. Rather, magma appears to be ponding at the base of the crust. As it solidifies, it releases a large quantity of water, which reduces *Vp*/*Vs*. This situation explains the lack of rhyolites in this region. Rhyolitic melts in the TVZ are partial melts of dominantly crustal origin, and thus require significant intrusion of the crust by partial melt. Why such intrusion has not yet occurred is most likely related to the greater pre-existing crustal thickness beneath Mt Ruapehu.

Forearc crust

The forearc crust is imaged as a relatively low *Vp*, high *Vp*/*Vs* region (Fig. 5). At shallow depth, *Vp* shows a good correlation with surface geology. *Vp* contours parallel the faults of both the east and west strands of the North Island dextral fault belt, with a particularly strong gradient in *Vp* along the west strand in Hawke's Bay (Figs 6a–b, near $x = 35, y = 0$). This strong gradient marks the transition from the Wairoa syncline in the southeast, which contains up to 5 km of post-Cretaceous sediments (Field *et al.* 1997), to the exposed Mesozoic greywacke basement of the axial ranges (Fig. 1). The Kaimanawa Mountains, which constitute the most extensive area of high topography in the North Island, are underlain by a region with $Vp > 6.0$ km s^{-1} at 4 km depth (centred near $x = -20, y = 25$ in Fig. 6b). This region retains a *Vp* close to 6 km s^{-1} down to 25 km depth. It is likely to represent a significant thickness of Haast schist, as discussed by Eberhart-Phillips *et al.* (2005). Its >20 km thickness suggests that it may act as a strong, coherent block within the forearc.

Vp/*Vs* is high throughout the forearc, and particularly at shallow depth (Figs 6a–c). Eberhart-Phillips *et al.* (1989) have shown *Vp*/*Vs* becomes high in sandstone when fluid pressure approaches lithostatic, porosity decreases or clay content increases. The high *Vp*/*Vs* we see most likely reflects overpressuring of the forearc, as this has been observed in exploration wells up to 4 km deep (Field *et al.* 1997; Allis *et al.* 1998). Sibson & Rowland (2003) argue that this overpressure stems partly from the abundance of low-permeability mudrocks in the forearc, and partly from the superior containment of overpressures by the compressional thrust-fault regime. In contrast, *Vp*/*Vs* beneath the Kaimanawa Mountains is low, suggesting hydrostatic conditions within this block. A feature of the *Vp*/*Vs* distribution is the sharp gradient across both strands of the North Island dextral fault belt, particularly across the west strand at 4 km depth east of the Kaimanawa Mountains (e.g. near $x = 35, y = 35$ in Fig. 6b). In terms of the fluid pressure regime, both these active fault strands are optimally located for strike-slip motion—they occur where σ_Z becomes σ_2 while changing from σ_3 to σ_1.

A distinct band of high *Vp*/*Vs* parallels the plate interface down to at least 40 km (Fig. 5). In the lower crust there is a one-to-one correspondence between the high *Vp*/*Vs* band and low *Vp* (Figs 6f–g). As this region lies above the upper plane of the dipping seismic zone and has $Vp < 6.5$ km s^{-1} at 32 km depth, it could represent a significant accumulation of underplated subducted sediment. If so, it could provide a viable mechanism for uplifting the Kaimanawa block. We lose resolution on this feature northeast of $y = -60$ and southwest of $y = 140$, particularly for *Vp*/*Vs*. However, previous seismic tomography results suggest that it continues to the northeast (Reyners *et al.* 1999), but pinches out to the southwest (Eberhart-Phillips *et al.* 2005).

A model for the distribution and productivity of magmatism in the central North Island

Outstanding questions on magmatism in the North Island include:

(1) *Why does magmatism not extend southwest of Mt Ruapehu?* The subducted plate extends at least 350 km to the southwest, where abundant seismicity in the dipping seismic zone extends to 230 km depth (Reyners & Robertson 2004). There has clearly been enough subduction in this region to expect magmatism.

(2) *Why is the modern central TVZ the most frequently active and productive silicic volcanic system on Earth?* Hochstein (1995)

has determined that the total crustal heat transfer of the TVZ is at present *ca.* 2600 MW/100 km along strike. Of this, only *ca.* 600 MW/100 km is a 'normal' subduction component—that is, associated with extrusions and intrusions of andesites and dacites. This leaves the bulk of the heat transfer to be explained by unusual mechanisms, such as the 'endogenous crustal heating' suggested by Hochstein (1995) to result from focussed plastic deformation within the ductile lithosphere of the Australian plate.

Our tomography results, when combined with other geophysical data, provide insights into both these questions. The answer to the first question lies in the marked variation in return flow in the mantle wedge along the strike of the subduction zone, as discussed earlier. The tomography suggests there is little return flow southwest of Mt Ruapehu, but well-developed return flow beneath the central TVZ. This pattern is well illustrated by Fig. 7(b), which shows the shallowest depth at which $Vp = 7.9$ km s^{-1}. Regions where this depth is >80 km indicate places where a large portion of the mantle wedge has low Vp—that is, where return flow is well developed. Extensive return flow is indicated northwest of the TVZ, and a smaller region of return flow is indicated northwest of Mt Taranaki. It is difficult to flux partial melt in the mantle without return flow, hence we would not expect magmatism southwest of Mt Ruapehu. Confirmation for such a marked change in mantle flow along strike comes from shear-wave splitting measurements from earthquakes in the dipping seismic zone (Audoine *et al.* 2004; Fig. 7b). These show a dramatic change in fast polarization direction from trench parallel southwest of Mt Ruapehu to trench perpendicular in the western TVZ. Lattice-preferred orientation of olivine generated by corner flow-induced strain within the mantle wedge is the most likely candidate for the fast polarization directions in the western TVZ. In contrast, the fast polarization directions to the southwest are more consistent with flow parallel to the subducted plate.

The answer to the second question requires mechanisms that provide an anomalous concentration of melt in the mantle, and thus an anomalous concentration of fluid to flux this melt. Our tomography results suggest two likely candidates for this:

(1) The subducted Hikurangi Plateau. Given that the thickness of the plateau is about twice that of normal oceanic crust, we would expect about twice the amount of fluid to be released from this crust as it dehydrates. Furthermore, the greater thermal time constant of this crust discussed previously may mean that the bulk of the fluid is released at greater depths than normal—possibly into the region of vigorous return flow rather than into the stagnant mantle nose. The effect of the Hikurangi Plateau will thus be to significantly increase the amount of partial melt in the mantle, compared to a normal subduction zone. However, it will not necessarily concentrate partial melt along strike, as is indicated by the low Vp, high Vp/Vs anomaly immediately northwest of Lake Taupo.

(2) Fluid flow along strike in the mantle. The abrupt cessation of corner flow southwest of Mt Ruapehu revealed by the tomography results is likely to cause lateral fluid flow in this region, as suggested by the shear-wave splitting results. In particular, we would expect the corner flow in the northeast to entrain fluid from the southwest. So the 'edge effect' of the termination of magmatism is itself leading to an anomalous concentration of partial melt, as fluid from a large volume of mantle to the southwest is available to flux melt. This situation is quite different from a normal subduction zone, where the along-arc variation of magmatism is often quite regular, pointing to uniform magma production along strike. For example, Quaternary volcanoes in the northeast Japan arc can be grouped into clusters striking transverse to the arc; these have an average width of 50 km,

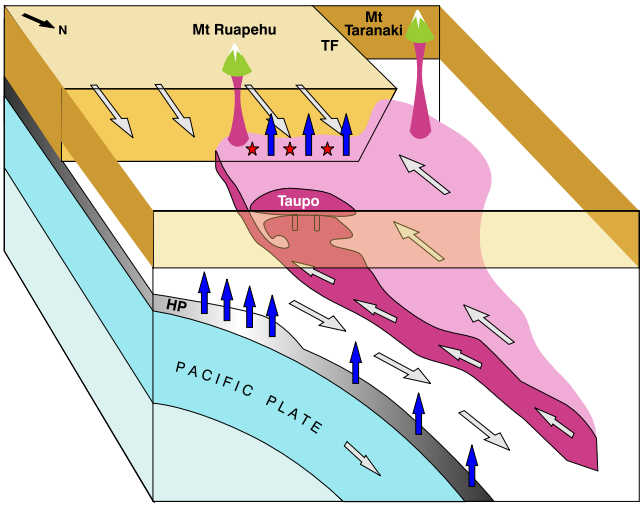

Figure 8. A schematic model for magmatism in the central North Island, viewed from the east–northeast. Grey arrows in the mantle wedge denote corner flow beneath the thinner crust northeast of Mt Ruapehu, and lateral mantle flow beneath the thicker crust southwest of Mt Ruapehu. The pink region denotes partial melt. Blue arrows show fluid flow, resulting from both dehydration of the subducting plate and solidification of ponded magma at the base of the thicker crust. Red stars are earthquakes in the lower crust. HP signifies the Hikurangi Plateau, and TF the Taranaki Fault. See text for further details.

and are separated by 30–75-km-wide volcanic gaps (Tamura *et al.* 2002). The anomalous concentration of partial melt inferred in the mantle wedge near the Taupo caldera arises because it is fluxed by fluid from an unusually long distance along strike.

Our model for magmatism in the central North Island is shown schematically in Fig. 8. The marked change in mantle return flow proposed at the southwestern termination of the TVZ implies a major change in the interaction between the mantle wedge, subducted slab and overriding plate. As pointed out by Eberle *et al.* (2002), in regions of well-developed mantle return flow, viscous decoupling occurs implicitly at shallow depth between the slab and the mantle wedge because hot material from the wedge is entrained close to the trench. We would thus expect a major change in the large-scale viscous coupling of the plates at the southwestern termination of the TVZ, from decoupled in the northeast to more strongly coupled to the southwest. Such a change in viscous coupling is likely to play a significant role in the long-term clockwise rotation of the forearc.

The magmatic system shown in Fig. 8 is unlikely to be stable long-term. It has long been assumed that the southern limit of the TVZ has been migrating southwestwards with time (e.g. Anderton 1981). Faulting characteristics and timing of the onset of faulting, together with the timing of recent volcanism in the southern TVZ, also suggest a southwestward propagation (Villamor & Berryman 2006). Our tomography results are consistent with such southwestward propagation—the locus of most active rhyolitic volcanism that we image (the Taupo caldera) lies at the southwestern limit of the rhyolite-dominated central section of the TVZ. This begs the question of how such propagation might be achieved, given the thicker crust to the southwest. The alignment of the northeastern boundary of this thick crust parallel to the backarc corner flow (Figs 6g and 7a) suggests that thermal erosion by this flow possibly plays a part. Our tomography results from the region of Mt Ruapehu allow us to speculate that this may be a two stage process—initial ponding of melt at the base of the crust, resulting in major weakening of

the crust by the large quantity of water released as the melt solidifies. The crust to the southwest of the TVZ is anomalous in a global sense, in that seismicity extends throughout the crust (Figs 5f–h). Wholesale weakening of the crust by fluid may explain this. We would thus interpret the concentration of seismicity just above the Moho along the northeastern edge of the thickened crust (Figs 6f and g) as due to anomalous amounts of fluid, rather than arising from the differential stresses set up at the junction of crustal columns of differing thickness, as suggested by Reyners (1989).

CONCLUDING REMARKS

In this paper we have used seismic tomography with a relatively coarse grid to constrain large-scale features associated with subduction and magmatism beneath the central North Island. The model for subduction and magmatism that we deduce from the tomography is put forward as the basis for further work. A planned 3-D inversion for seismic attenuation should provide more information on the rheology and temperature distribution within the mantle wedge, and serve to constrain the model.

Also, more detailed studies are planned with the data, especially for the shallow part of the plate interface, and for the crust in the backarc.

ACKNOWLEDGMENTS

The CNIPSE experiment would not have been possible without the support of landowners in the central North Island, and we thank them for their enthusiasm. Peter McGinty, Fred Langford, Steve Sherburn, Dave Francis and Michael Bourne are particularly thanked for their sterling efforts in the field. Thanks are also due to Martha Savage of Victoria University of Wellington and Daniel Rowlands of the University of Cambridge for data exchange. Russell Robinson, Tony Hurst and two anonymous reviewers are thanked for thorough reviews of the manuscript. This research has been supported by the New Zealand Foundation for Research, Science & Technology, the School of Earth Sciences of the University of Leeds, The Royal Society of London and the Japan Science and Technology Agency.

REFERENCES

Allis, R.G., Funnell, R. & Zhan, X., 1998. From basin to mountains and back again: NZ basin evolution since 10 Ma, *WRI9—Proc. 9th Int. Symp. on Water-Rock Interaction*, Taupo, NZ, 30 March-3 April, pp. 3–9. A.A. Balkema, Rotterdam.

Anderson, H. & Webb, T., 1994. New Zealand seismicity: patterns revealed by the upgraded National Seismograph Network, *N. Z. J. Geol. Geophys.,* **37,** 477–493.

Anderton, P.W., 1981. Structure and evolution of the South Wanganui Basin, New Zealand, *N. Z. J. Geol. Geophys.,* **24,** 39–63.

Ansell, J.H. & Bannister, S.C., 1996. Shallow morphology of the subducted Pacific plate along the Hikurangi margin, New Zealand, *Phys. Earth planet. Inter.,* **93,** 3–20.

Audoine, E., Savage, M.K. & Gledhill, K., 2004. Anisotropic structure under a back-arc spreading region, the Taupo Volcanic Zone, New Zealand, *J. geophys. Res.,* **109,** B11305, doi:10.1029/2003JB002932.

Bannister, S., Bryan, C.J. & Bibby, H.M., 2004. Shear wave velocity variation across the Taupo Volcanic Zone, New Zealand, from receiver function inversion, *Geophys. J. Int.,* **159,** 291–310.

Beanland, S., 1995. The North Island Dextral Fault Belt, Hikurangi subduction margin, New Zealand, *PhD thesis,* Victoria Univ. of Wellington.

Bibby, H.M., Caldwell, T.G., Davey, F.J. & Webb, T.H., 1995. Geophysical evidence on the structure of the Taupo volcanic zone and its hydrothermal circulation, *J. Volc. Geotherm. Res.,* **68,** 29–58.

Boddington, T., Parkin, C.J. & Gubbins, D., 2004. Isolated deep earthquakes beneath the North Island of New Zealand, *Geophys. J. Int.,* **158,** 972–982.

Buland, R. & Chapman, C.H., 1983. The computation of seismic travel times, *Bull. seism. Soc. Am.,* **73,** 1271–1301.

Carter, R.M. & Naish, T.R., 1999. The high-resolution chronostratigraphic and sequence stratigraphic record of the Plio-Pleistocene, Wanganui Basin, New Zealand, *Inst. Geological & Nuclear Sci. Folio Series 2*, Lower Hutt, New Zealand.

Cashman, S.M., Kelsey, H.M., Erdman, C.F., Cutten, H.N.C. & Berryman, K.R., 1992. Strain partitioning between structural domains in the forearc of the Hikurangi subduction zone, New Zealand, *Tectonics,* **11,** 242–257.

Chadwick, M.P., 1997. The 1991 Hikurangi margin seismic refraction experiment, *PhD thesis,* Victoria Univ. of Wellington, New Zealand.

Chatterjee, S.N., Pitt, A.M. & Iyer, H.M., 1985. *Vp*/*Vs* ratios in the Yellowstone national park region, Wyoming, *J. Volc. Geotherm. Res.,* **26,** 213–230.

Chiu, J.M., Steiner, G., Smalley, R. & Johnston, A.C., 1991. PANDA: a simple, portable seismic array for local- to regional-scale seismic experiments, *Bull. seism. Soc. Am.,* **81,** 1000–1014.

Christensen, N.I., 1996. Poisson's ratio and crustal seismology, *J. geophys. Res,* **101,** 3139–3156.

Darby, D.J. & Meertens, C.M., 1995. Terrestrial and GPS measurements of deformation across the Taupo back arc and Hikurangi forearc regions in New Zealand, *J. geophys. Res,* **100,** 8221–8232.

Davy, B. & Collot, J.-Y., 2000. The Rapuhia Scarp (northern Hikurangi Plateau)—its nature and subduction effects on the Kermadec Trench, *Tectonophysics,* **328,** 269–295.

Davy, B. & Wood, R., 1994. Gravity and magnetic modelling of the Hikurangi Plateau, *Marine Geology,* **118,** 139–151.

DeMets, C., Gordon, R.G., Argus, D.F. & Stein, S., 1994. Effect of recent revisions to the geomagnetic reversal time scale on estimates of current plate motions, *Geophys. Res. Lett.,* **21,** 2191–2194.

Dziewonski, A.M. & Anderson, D.L., 1981. Preliminary Reference Earth Model, *Phys. Earth planet. Inter.,* **25,** 297–356.

Eberhart-Phillips, D., 1986. Three-dimensional velocity structure in Northern California Coast Ranges from inversion of local earthquake arrival times, *Bull. seism. Soc. Am.,* **76,** 1025–1052.

Eberhart-Phillips, D., 1990. Three-dimensional P- and S-velocity structure in the Coalinga region, California, *J. geophys. Res,* **95,** 15 343–15 363.

Eberhart-Phillips, D., 1993. Local earthquake tomography: earthquake source regions, in *Seismic Tomography: Theory and Practice*, pp. 613–643, eds Iyer, H.M. & Hirahara, K., Chapman and Hall, London.

Eberhart-Phillips, D. & Michael, A.J., 1998. Seismotectonics of the Loma Prieta, California, region determined from three-dimensional Vp, Vp/Vs, and seismicity, *J. geophys. Res.,* **103,** 21 099–21 120.

Eberhart-Phillips, D. & McVerry, G., 2003. Estimating slab earthquake response spectra from a 3D *Q* model, *Bull. seism. Soc. Am.,* **93,** 2649–2663.

Eberhart-Phillips, D., Han, D-H. & Zoback, M.D., 1989. Empirical relationships among seismic velocity, effective pressure, porosity, and clay content in sandstone, *Geophysics,* **54,** 82–89.

Eberhart-Phillips, D., Christensen, D.H., Brocher, T.M., Dutta, U., Hansen, R. & Ratchkovski, N.A., 2003. Imaging the transition from Aleutian subduction to Yakutat collision in central Alaska, with local earthquakes and active source data, *EOS, Trans. Am. geophys. Un.,* **84**(46), Fall Meet. Suppl., Abstract S21C-01.

Eberhart-Phillips, D., Reyners, M., Chadwick, M. & Chiu, J-M., 2005. Imaging subduction zone coupling: 3-D *Vp*, *Vp*/*Vs* and *Q* in the southern North Island, New Zealand, *Geophys. J. Int.,* **162,** 270–288.

Eberle, M.A., Grasset, O. & Sotin, C., 2002. A numerical study of the interaction between the mantle wedge, subducting slab, and overriding plate, *Phys. Earth planet. Inter.,* **134,** 191–202.

Field, B.D., Uruski, C.I. & others, 1997. Cretaceous-Cenozoic geology and petroleum systems of the East Coast Region, New Zealand, *Inst. Geological & Nuclear Sci. Monograph 19*, Lower Hutt, New Zealand.

Galea, P., 1992. Observations of very high *P*-velocities in the subducted slab, New Zealand, and their relation with slab geometry, *Geophys. J. Int.,* **110,** 238–250.

Hacker, B.R., Abers, G.A. & Peacock, S.M., 2003a. Subduction factory 1. Theoretical mineralogy, densities, seismic wave speeds, and H2O contents, *J. geophys. Res.,* **108,** 2029, doi:10.1029/2001JB001127.

Hacker, B.R., Peacock, S.M., Abers, G.A. & Holloway, S.D., 2003b. Subduction factory 2. Are intermediate-depth earthquakes in subducting slabs linked to metamorphic dehydration reactions?, *J. geophys. Res.,* **108,** 2030, doi:10.1029/2001JB001129.

Harrison, A.J. & White, R.S., 2004. Crustal structure of the Taupo Volcanic Zone, New Zealand: stretching and igneous intrusion, *Geophys. Res. Lett.,* **31,** L13615, doi: 10.1029/2004GL019885.

Hasegawa, A. & Nakajima, J., 2004. Geophysical constraints on slab subduction and arc magmatism, in The State of the Planet: Frontiers and Challenges in Geophysics, *Geophys. Monogr. Ser.,* **150,** 81–94, AGU, Washington, DC.

Henrys, S., Reyners, M. & Bibby, H., 2003a. Exploring the plate boundary structure of New Zealand, *EOS, Trans. Am. geophys. Un.,* **84,** 289, 294–295.

Henrys, S. *et al.*, 2003b. New Zealand North Island GeopHysical Transect (NIGHT): field acquisition report, *Inst. Geological & Nuclear Sci. Science Report* 2003/19, Lower Hutt, New Zealand.

Hochstein, M.P., 1995. Crustal heat transfer in the Taupo Volcanic Zone (New Zealand): comparison with other volcanic arcs and explanatory heat source models, *J. Volc. Geotherm. Res.,* **68,** 117–151.

Hoernle, K., Hauff, F., Werner, R., Mortimer, N., van den Bogaard, P., Geldmacher, J. & Garbe-Schoenberg, D., 2004. Geochemical evolution of the Hikurangi oceanic plateau, New Zealand, *EOS, Trans. Am. geophys. Un.,* **85**(47), Fall Meeting Suppl., Abstract V51B-0574.

Hyndman, R.D., Yamano, M. & Oleskevich, D.A., 1997. The seismogenic zone of subduction thrust faults, *Island Arc,* **6,** 244–260.

Ji, S. & Wang, Z., 1999. Elastic properties of forsterite-enstatite composites up to 3.0 GPa. *J. Geodyn.,* **28,** 147–174.

Karato, S., 2003. Mapping water content in the upper mantle, in *Inside the subduction factory, Geophysical Monograph*, Vol. 138, pp. 135–152, ed. Eiler, J., AGU, Washington D.C.

Kincaid, C. & Sacks, I.S., 1997. Thermal and dynamical evolution of the upper mantle in subduction zones, *J. geophys. Res.,* **102,** 12 295–12 315.

Kirby, S., Engdahl, E.R. & Denlinger, R., 1996. Intermediate-depth intraslab earthquakes and arc volcanism as physical expressions of crustal and uppermost mantle metamorphism in subducting slabs, in *Subduction top to bottom*, Vol. 96, pp. 195–214, eds Bebout, G.E. *et al.*, Amer. Geophys. Union Geophys. Monograph.

Kissling, E., Ellsworth, W.L., Eberhart-Phillips, D. & Kradolfer, U., 1994. Initial reference models in seismic tomography, *J. geophys. Res.,* **99,** 19 635–19 646.

Lewis, K. & Pettinga, J., 1993. The emerging, imbricate frontal wedge of the Hikurangi margin, in *South Pacific Sedimentary Basins of the World*, pp. 225–250, ed. Ballance, P.F., Elsevier, Amsterdam.

Michelini, A., 1991. Fault zone structure determined through the analysis of earthquake arrival times, *PhD thesis,* Univ. Calif., Berkeley, California.

Michelini, A. & McEvilly, T.V., 1991. Seismological studies at Parkfield: I. Simultaneous inversion for velocity structure and hypocenters using cubic b-splines parameterization, *Bull. seism. Soc. Am.,* **81,** 524–552.

Mortimer, N., 2004. New Zealand's Geological Foundations, *Gondwana Res.,* **7,** 261–272.

Mortimer, N. & Parkinson, D., 1996. Hikurangi plateau: a cretaceous large igneous province in the southwest Pacific Ocean, *J. geophys. Res.,* **101,** 687–696.

Nakajima, J. & Hasegawa, A., 2003. Estimation of thermal structure in the mantle wedge of northeastern Japan from seismic attenuation data, *Geophys. Res. Lett.,* **30,** 1760, doi: 10.1029/2003GL017185.

Nakajima, J., Matsuzawa, T., Hasegawa, A. & Zhao, D., 2001a. Three-dimensional structure of *Vp*, *Vs*, and *Vp*/*Vs* beneath northeastern Japan: implications for arc magmatism and fluids, *J. geophys. Res.,* **106,** 21 843–21 857.

Nakajima, J., Matsuzawa, T., Hasegawa, A. & Zhao, D., 2001b. Seismic imaging of arc magma and fluids under the central part of northeastern Japan, *Tectonophysics,* **341,** 1–17.

Nicol, A., Van Dissen, R., Vella, P., Alloway, B. & Melhuish, A., 2002. Growth of contractional structures during the last 10 m.y. at the southern end of the emergent Hikurangi forearc basin, New Zealand, *N. Z. J. Geol. Geophys.,* **45,** 365–385.

Nicol, A., Stagpoole, V. & Maslen, G., 2004. Structure and petroleum potential of the Taranaki fault play, *New Zealand Petroleum Conference Proceedings*, 7–10 March 2004.

Pulford, A. & Stern, T., 2004. Pliocene exhumation and landscape evolution of central North Island, New Zealand: the role of the upper mantle, *J. geophys. Res.,* **109,** F01016, doi:10.1029/2003JF000046.

Reilly, W.I., 1973. A conformal mapping projection with minimum scale error, *Survey Review,* **22,** 57–71.

Reyners, M., 1980. A microearthquake study of the plate boundary, North Island, New Zealand, *Geophys. J. R. astr. Soc.,* **63,** 1–22.

Reyners, M., 1989. New Zealand seismicity 1964–87: an interpretation, *N.Z. J. Geol. Geophys.,* **32,** 307–315.

Reyners, M., 1998. Plate coupling and the hazard of large subduction thrust earthquakes at the Hikurangi subduction zone, New Zealand, *N.Z. J. Geol. Geophys.,* **41,** 343–354.

Reyners, M. & Robertson, E. de J., 2004. Intermediate depth earthquakes beneath Nelson, New Zealand, and the southwestern termination of the subducted Pacific plate, *Geophys. Res. Lett.,* **31,** L04607, doi: 10.1029/2003GL019201.

Reyners, M. & Stuart, G., 2002. The central North Island passive seismic experiment, *Inst. Geological & Nuclear Sci. Science Report* 2002/11, Lower Hutt, New Zealand.

Reyners, M., Eberhart-Phillips, D. & Stuart, G., 1999. A three-dimensional image of shallow subduction: crustal structure of the Raukumara Peninsula, New Zealand, *Geophys. J. Int.,* **137,** 873–890.

Robinson, R., Smith, E.G.C. & Latter, J.H., 1981. Seismic studies of the crust under the hydrothermal areas of the Taupo Volcanic Zone, New Zealand, *J. Volc. Geotherm. Res.,* **9,** 253–267.

Salmon, M., Bannister, S., Bibby, H., Savage, M. & Stern, T., 2003. Attenuation and electrical resistivity in an asymmetric back arc extensional environment, *EOS, Trans. Am. geophys. Un.,* **84**(46), Fall Meet. Suppl., Abstract S22B-0450.

Sato, H., Sacks, I.S., Murase, T., Muncill, G. & Fukuyama, H., 1989. *Qp*-melting temperature in peridotite at high pressure and temperature: attenuation mechanism and implications for the mechanical properties of the upper mantle, *J. geophys. Res.,* **94,** 10 647–10 661.

Sherburn, S. & White, R.S., 2005. Crustal seismicity in Taranaki, New Zealand using accurate hypocentres from a dense network, *Geophys. J. Int.,* **162,** 494–506.

Sherburn, S., Bannister, S. & Bibby, H., 2003. Seismic velocity structure of the central Taupo Volcanic Zone, New Zealand, from local earthquake tomography, *J. Volc. Geotherm. Res.,* **122,** 69–88.

Sibson, R.H. & Rowland, J.V., 2003. Stress, fluid pressure and structural permeability in seismogenic crust, North Island, New Zealand, *Geophys. J. Int.,* **154,** 584–594.

Stern, T.A. & Davey, F.J., 1989. Crustal structure and origin of basins formed behind the Hikurangi subduction zone, New Zealand, in *Origin and evolution of sedimentary basins and their energy and mineral resources, Geophysical Monograph*, Vol. 48, pp. 73–85, ed. Price, R.A., Amer. Geophys. Union.

Stern, T.A., Smith, E.G.C., Davey, F.J. & Muirhead, K.J., 1987. Crustal and upper mantle structure of the northwestern North Island, New Zealand, from seismic refraction data, *Geophys. J. R. astr. Soc.,* **91,** 913–936.

Stern, T.A., Quinlan, G.M. & Holt, W.E., 1992. Basin formation behind an active subduction zone: three-dimensional flexural modelling of Wanganui Basin, New Zealand, *Basin Res.,* **4,** 197–214.

Stratford, W.R. & Stern, T.A., 2004. Strong seismic reflections and melts in the mantle of a continental back-arc basin, *Geophys. Res. Lett.,* **31,** L06622, doi: 10.1029/2003GL019232.

Takei, Y., 2002. Effect of pore geometry on Vp/Vs: from equilibrium geometry to crack, *J. geophys. Res.,* **107**(B2), 2043, doi:10.1029/2001JB000522.

Tamura, Y., Tatsumi, Y., Zhao, D., Kido, Y. & Shukono, H., 2002. Hot fingers in the mantle wedge: new insights into magma genesis in subduction zones, *Earth planet. Sci. Lett.,* **197,** 105–116.

Tatsumi, Y., 1989. Migration of fluid phases and genesis of basalt magmas in subduction zones, *J. geophys. Res.,* **94,** 4697–4707.

Thurber, C.H., 1983. Earthquake locations and three-dimensional crustal structure in the Coyote Lake area, central California, *J. geophys. Res.,* **88,** 8226–8236.

Thurber, C.H., 1993. Local earthquake tomography: velocities and Vp/Vs - theory, in *Seismic Tomography: Theory and Practice*, pp. 563–583, ed. Iyer, H.M. & Hirahara, K., Chapman and Hall, London.

Ulmer, P. & Trommsdorff, V., 1995. Serpentine stability to mantle depths and subduction-related magmatism, *Science,* **268,** 858–861.

Villamor, P. & Berryman, K., 2001. A late Quaternary extension rate in the Taupo Volcanic Zone, New Zealand, derived from fault slip data, *N.Z. J. Geol. Geophys.,* **44,** 243–269.

Villamor, P. & Berryman, K., 2006. Evolution of the southern termination of the Taupo Rift, New Zealand, *N.Z. J. Geol. Geophys.*, **49,** 23–37.

Wallace, L., Beavan, J., McCaffrey, R. & Darby, D., 2004. Subduction zone coupling and tectonic block rotations in the North Island, New Zealand, *J. geophys. Res.,* **109,** B12406, doi:10.1029/2004JB003241.

Wiemer, S. & Benoit, J.P., 1996. Mapping the b-value anomaly at 100 km depth in the Alaska and New Zealand subduction zones, *Geophys. Res. Lett.,* **23,** 1557–1560.

Wiens, D.A. & Smith, G.P., 2003. Seismological constraints on structure and flow patterns within the mantle wedge, in *Inside the subduction factory, Geophysical Monograph*, Vol. 138, pp. 59–81, ed. Eiler, J., AGU, Washington DC.

Wilson, C.J.N., Houghton, B.F., McWilliams, M.O., Lanphere, M.A., Weaver, S.D. & Briggs, R.M., 1995. Volcanic and structural evolution of Taupo Volcanic Zone, New Zealand: a review, *J. Volc. Geotherm. Res.,* **68,** 1–28.

Wilson, C.J.N., Blake, S., Charlier, B.L.A. & Sutton, A.N., 2006. The 26.5 ka Oruanui eruption, Taupo volcano, New Zealand: development, characteristics and evacuation of a large rhyolite magma body, *J. Petrol.,* **47,** 35–69.

Yamasaki, T. & Seno, T., 2003. Double seismic zone and dehydration embrittlement of the subducting slab, *J. geophys. Res.,* **108**(B4), 2212, doi:10.1029/2002JB001918.

Zhang, H., Thurber, C.H., Shelly, D., Ide, S., Beroza, G.C. & Hasegawa, A., 2004. High-resolution subducting-slab structure beneath northern Honshu, Japan, revealed by double-difference tomography. *Geology,* **32,** 361–364.